

1 **A sea surface temperature reconstruction for the southern Indian**
2 **Ocean trade wind belt from corals in Rodrigues Island (19°S, 63°E)**

3

4 J. Zinke^{1,2,3,4}, L. Reuning⁵, M. Pfeiffer⁵, J. Wassenburg⁶, E. Hardman⁷, R. Jhangeer-
5 Khan⁷, Davies, G. R.⁸, C.K.C. Ng⁹, and D. Kroon¹⁰

6

7 ¹Division of Paleontology, Freie Universitaet Berlin, Malteserstrasse 74-100, Berlin,
8 12249, Germany

9 ²Department of Environment and Agriculture, Curtin University of Technology, Kent
10 Street, Bentley, WA6102, Australia

11 ³Australian Institute of Marine Science, Nedlands, WA 6009, Australia

12 ⁴School of Geography, Archaeology and Environmental Studies, University of
13 Witwatersrand, Johannesburg, South Africa.

14 ⁵Geological Institute, RWTH Aachen, Wuellnerstrasse2, 52056 Aachen, Germany

15 ⁶Institute for Geosciences, Johannes-Gutenberg-University Mainz, Johann-Joachim-
16 Becher-Weg 21, D-55128 Mainz

17

18 ⁷SHOALS Rodrigues, Rodrigues, Mauritius

19 ⁸Geology & Geochemistry, VU University Amsterdam, De Boelelaan 1085, 1081 HV
20 Amsterdam, Netherlands

21 ⁹Department of Medical Radiation Sciences, Curtin University of Technology, Kent
22 Street, Bentley, WA6102, Australia

23 ¹⁰University of Edinburgh, School of GeoSciences, The King's Buildings, West Mains
24 Road, Edinburgh EH9 3JW, UK.

25

26 **Correspondence to:** Jens Zinke, jens.zinke@gmail.com

27

28 **Abstract**

29 The western Indian Ocean has been warming rapidly over recent decades causing a
30 greater number of extreme climatic events. It is therefore of paramount importance to
31 improve our understanding of links between Indian Ocean sea surface temperature (SST)
32 variability, climate change, and sustainability of tropical coral reef ecosystems. Here we
33 present monthly-resolved coral Sr/Ca records from two different locations from
34 Rodrigues Island (63°E, 19°S) in the south-central Indian Ocean trade wind belt. We
35 reconstruct SST based on a linear relationship with the Sr/Ca proxy with records starting
36 from 1781 and 1945, respectively. We assess relationships between the observed long-
37 term SST and climate fluctuations related to the El Nino-Southern Oscillation (ENSO),
38 the Subtropical Indian Ocean Dipole Mode (SIOD) and the Pacific Decadal Oscillation
39 (PDO) between 1945 and 2006, respectively. The reproducibility of the Sr/Ca records are
40 assessed as are the potential impacts of diagenesis and corallite orientation on Sr/Ca-SST
41 reconstructions. We calibrate individual robust Sr/Ca records with *in-situ* SST and
42 various gridded SST products. The results show that the SST record from Cabri provides
43 the first Indian Ocean coral proxy time series that records the SST signature of the PDO
44 in the south-central Indian Ocean since 1945. We suggest that additional records from
45 Rodrigues Island can provide excellent records of SST variations in the southern Indian
46 Ocean trade wind belt to unravel teleconnections with the SIOD/ENSO/PDO on longer
47 time scales.

48

49 **1 Introduction**

50 The Indian Ocean has been warming steadily over the past century with the western
51 portion of the basin having experienced an increase in SST of up to 1.2°C over the past
52 60 years (Koll Roxy et al., 2014). The Indian Ocean has also taken up a large amount of
53 heat in its interior between 1999 and 2016 when global SST increased at a smaller rate
54 compared to previous decades (Lee et al., 2015). The strong Indian Ocean warming over
55 the past century is thought to have contributed to a decreasing land-sea thermal contrast
56 with the Indian subcontinent affecting monsoon rainfall and potentially playing a major
57 role in the decrease in East African rainfall between March to May in recent decades
58 (Funk et al., 2008; Koll Roxy et al., 2015). The western Indian Ocean warming has also
59 been shown to follow closely anthropogenic radiative forcing over the past century (Funk
60 et al., 2008; Alory et al., 2009; Koll Roxy et al., 2015). Furthermore, the western Indian
61 Ocean warmed significantly during past El Niño events with the 1997/98 event causing
62 widespread coral bleaching and mortality (Sheppard, 2003). Synchronously, intrinsic
63 climate modes to the Indian Ocean, like the Subtropical Indian Ocean Dipole Mode
64 during austral summer (SIOD; Fig. 1b; Behera and Yamagata, 2001; Reason, 2001), can
65 interfere with the Indian Ocean-wide teleconnections in SST and rainfall caused by the El
66 Niño-Southern Oscillation (ENSO) or behave independently (Hoell et al., 2016).
67 Mounting evidence indicates that the Pacific Decadal Oscillation (PDO) or Pacific
68 Decadal Variability (PDV) has teleconnections extending to the western Indian Ocean
69 (Fig. 1c; Cole et al., 2000; Crüger et al., 2009). The positive PDO phase corresponds to
70 warm western Indian Ocean SST anomalies (Fig. 1c; Deser et al., 2004), thought to
71 exceed SST anomalies associated with ENSO (Krishnan and Sugi, 2003), particularly in

72 the southwestern Indian Ocean (Meehl and Hu, 2006). It is therefore of paramount
73 importance to improve our understanding of links between Indian Ocean SST variability,
74 global climate change, and sustainability of tropical coral reef ecosystems. Yet, long-term
75 observational records of Indian Ocean SST are sparse and are thought to be only reliable
76 after the 1960's (Tokinaga et al., 2012).

77 Paleoclimate reconstructions of SST from massive corals have provided
78 invaluable records for past SST trends and interannual to decadal variability in the
79 western Indian Ocean (Charles et al., 1997; Cole et al., 2000; Cobb et al., 2001; Pfeiffer
80 et al., 2004, 2009; Pfeiffer & Dullo, 2006; Nakamura et al., 2009; Crueger et al., 2009;
81 Grove et al., 2013a, b; Zinke et al. 2008, 2009, 2014). Massive corals, such as *Porites*
82 spp., can grow for centuries at a rate of 0.5 and 2 cm.yr⁻¹. Therefore, down-core
83 geochemical sampling of massive corals can yield reconstructed SST time series at
84 approximately monthly resolution. As the coral precipitates its skeleton, trace elements
85 and stable isotopes are incorporated in proportion to ambient SSTs (Felis and Pätzold,
86 2003). Both, the Sr/Ca ratio and $\delta^{18}\text{O}$ composition of the coral aragonite have been shown
87 to be reliable paleo-thermometers with a negative relationship with SST (Alibert and
88 McCulloch, 1997; Pfeiffer & Dullo, 2006; DeLong et al., 2012). A compilation of Sr/Ca-
89 SST calibrations for *Porites spp.* revealed a mean Sr/Ca relationship with SST of -
90 0.061mmol/mol/1°C SST increase (Corrège, 2006). Since Sr has a long oceanic residence
91 time, skeletal Sr/Ca is assumed to mainly reflect SST variability. The quality and
92 accuracy of paleo-thermometers strongly depends on optimal sampling of the major
93 growth axes (De Long et al., 2012). Furthermore, diagenetic alterations of coral aragonite
94 can lead to errors in SST reconstructions and it is important that this effect is identified

95 and excluded based on petrographic analysis (McGregor and Gagan, 2003; Hendy et al.,
96 2007; McGregor and Abram, 2008; Sayani et al., 2011; Smodej et al., 2015).

97 Currently, none of the coral proxy records from the western Indian Ocean cover
98 the south-central Indian Ocean basin in the heart of the trade wind system and the
99 Suptropical Indian Ocean Dipole Mode (Fig. 1b). Furthermore, all proxy records of
100 interest for the trade wind belt are based on oxygen isotopes with the exception of two
101 Sr/Ca ratio records covering 1963 to 2008 from St. Marie Island off East Madagascar
102 (Grove et al., 2013a). The latter provided mixed results with discrepancies in terms of the
103 long-term SST trend estimates due to the confounding effects of coral calcification in at
104 least one core (Grove et al., 2013a). A coral oxygen isotope record from Reunion Island
105 (21°S, 55°E; Mascarene Islands) located approximately 230km to the southwest of
106 Mauritius spans the period 1832 to 1994 and is the longest for the subtropical region off
107 East Madagascar (Pfeiffer et al., 2004). Pfeiffer et al. (2004) showed evidence that the La
108 Reunion coral dominantly recorded past variation in salinity associated with transport
109 changes of the South Equatorial Current. The proxy time series records decadal
110 anomalies that were opposite to those of SST. Crüger et al. (2009) reported close linkages
111 of the salinity, sea-level pressure (SLP) and SST signal associated with the Pacific
112 Decadal Oscillation (Mantua et al., 1997) in coral records from Reunion and Ifaty (SW
113 Madagascar), respectively. Two coral oxygen isotope records from the Seychelles located
114 in the tropical western Indian Ocean (5°S, 54°E) were interpreted as an excellent record
115 of past Southwest Monsoon SST changes and showed significant correlations with air
116 temperatures over India between 1847 to 1994 (Charles et al., 1997; Pfeiffer & Dullo,
117 2006). Both, the Reunion and Seychelles records record strong correlations with the

118 ENSO on interannual and decadal time scales (Pfeiffer & Dullo, 2006). Although the
119 PDO also has a strong impact on the SST in the southwest Indian Ocean (Fig. 1c;
120 Krishnan and Sugi, 2003; Deser et al., 2004), the SST signature of the PDO has not
121 been reported in coral records from this region to date.

122 Here, we aim to reconstruct past SSTs from Sr/Ca ratios in two coral cores
123 obtained from Rodrigues Island (19°S, 63°E) located 690 km to the North-East of
124 Mauritius within the trade wind belt of the south-central Indian Ocean. To obtain a robust
125 SST record, we assess the reproducibility of the Sr/Ca proxy, and provide a rigorous
126 assessment of the potential impacts of diagenesis and corallite orientation on Sr/Ca-SST
127 reconstructions. We calibrate individual Sr/Ca records with *in-situ* SST and various
128 gridded SST products and verify the suitability of SST products for climate studies in the
129 south-central Indian Ocean. Furthermore, we assess relationships between the observed
130 long-term SST and climate fluctuations related to the ENSO, the SIOD and the PDO
131 between 1945 and 2006, respectively.

132

133 **2 Regional setting and climate**

134 Rodrigues (63°E, 19°S) is a small volcanic island in the southern Indian Ocean, about
135 619 km east of Mauritius (Fig. 1). It is part of the eastern edge of the Mascarene Plateau
136 that comprises Lower Tertiary basalts (Mart 1988) formed by a seaward flow of lava,
137 which has been eroded by hydrodynamic forces, and biological and chemical processes
138 (Turner and Klaus, 2005). Rodrigues has a surface area of about 119 km², with a
139 maximum altitude of 396 meter above sea level and is surrounded by a nearly continuous
140 fringing reef approximately 90 km in length (Turner and Klaus, 2005; Lynch et al. 2002).

141 The reef encloses a shallow lagoon, which, at 240km², is twice the area of the island
142 itself. The maximum tidal range is approximately 1.5m, and since the average water
143 depth in the lagoon is less than 2m, some areas are exposed at low spring tides. The water
144 depth immediately beyond the reef slopes is usually within the range of 10m to 30m. The
145 island has three major channels, one dredged for the main harbour at Port Mathurin in the
146 north, and natural channels in the south near Port Sud Est and in the East at St Francois.
147 Several small passes are also found around the reef (Turner and Klaus, 2005).

148 The water surrounding Rodrigues is supplied by the South Equatorial Current (SEC)
149 (New et al., 2005, 2007), a broad east to west current between 10° and 20° S in the Indian
150 Ocean driven by the southeast trade winds (Schott and McCreary, 2001). The southern
151 part of the SEC water flows in several directions past Rodrigues in southwest and
152 southeast direction, and westward to Mauritius (New et al., 2005, 2007).

153 Rodrigues has a relatively dry climate and annual mean evaporation exceeds
154 precipitation. Yearly precipitation is ~1000 mm mostly from January to April related to
155 the position of the Inter Tropical Convergent Zone (ITCZ). Between November and
156 March, the Southern Indian Ocean is affected by tropical cyclones, as a result of warm
157 SSTs and a strong convergence between northeast and southeast trades. Rodrigues
158 experiences two to sixteen cyclones per year, of which 2.5 are extreme (category 3 and
159 higher) with winds of 280 km/h and storm surges that reach 100 m inland and 2 m above
160 sea level. They usually last five to ten days (Turner and Klaus, 2005).

161 SST was monitored hourly *in situ* by a conductivity, temperature and depth (CTD)
162 device 150m offshore from the northern fringing reefs at Totor between 2002 to 2006
163 (Hardman et al., 2004, 2008). Maximum SST are recorded between December to March

164 (28.6 ± 0.5°C) and minimum SST between July to September (22.4 ± 0.27°C). Annual
165 mean SST is 25.49 ± 0.24°C with a seasonal amplitude of 6.22 ± 0.68°C.

166 Air temperatures have been recorded by the WMO weather station 61988 (name:
167 Rodrigues, Mauritius) located at the northern coast of Rodrigues since 1951 and are
168 available at <http://climexp.knmi.nl/>. The most recent years between 1997 and 2007 have
169 been provided by the Rodrigues Meteorological Office. The warmest months are
170 December to March (31.2 ± 0.3°), the coldest months are July to September (24.2 ± 0.3°).
171 Yearly average air temperature is 27.49°C ± 0.31°C with a yearly amplitude of about 7 ±
172 0.79°C.

173

174 **3 Materials and Methods**

175 Two coral cores were drilled from massive, dome-shaped *Porites* sp. and *Porites*
176 *lobata* at the northern reef sites Totor and Cabri, respectively (Fig. 1; Table 1). The size
177 of the coral colonies at Totor is ~2.5m and that of Cabri is ~4m in height. Both colonies
178 were healthy and showed no signs of disease or dead surfaces at the time of drilling. The
179 220cm long Totor core was obtained in August 2005 from the forereef slope of the
180 northern fringing reef facing the open ocean with the top of the colony at 4m water depth.
181 The 180cm long Cabri core was obtained in March 2007 growing in 3m water depth
182 about 1km to the northeast of Totor from the outer fringing reef at Passe Cabri. The site
183 Cabri is more exposed to trade winds as compared to Totor that is more sheltered
184 (Hardman et al., 2004, 2008).

185 A commercially available pneumatic drill driven by scuba tanks was used to
186 extract cores along the central growth axis, with a diameter measuring 4 cm. Cores were

187 sectioned into 7 mm thick slabs, rinsed several times with demineralised water, cleaned
188 with compressed air to remove any surficial particles and dried for more than 24 hours in
189 a laminar flow hood. Annual density bands were visualised by X-radiograph-positive
190 prints, and the growth axis of the coral slab was defined as the line normal to these
191 laminae (Figs. A4 and A5). Coral densities (g/cm^3) were calculated by analysing digital
192 X-rays using the program CoralXDS and densitometry (Fig. S1; Helmle et al., 2011;
193 Carricart-Ganivet et al., 2007), calcification rate ($\text{g}/\text{cm}^2 \text{yr}^{-1}$) by multiplying density with
194 extension rate. The annual extension rates (cm yr^{-1}) were calculated by measuring the
195 distance (cm) between density minima using the program CoralXDS (Fig. S1). With a
196 diamond coated drill mounted on top of a movable support frame, samples were taken
197 every 1 mm parallel to the growth axis, equivalent to approximately monthly resolution.

198 A combination of X-ray images, X-ray diffraction (XRD), light and scanning
199 electron microscopy (SEM) with Energy Dispersive X-Ray Spectrometer (EDS) was used
200 to investigate possible diagenetic alteration in the Totor and Cabri cores. All core sections
201 from both Totor and Cabri were initially screened for diagenetic alterations using X-ray
202 images (Appendix Figs. 4 and 5). Corals that showed an annual density banding without
203 anomalous high or low density patches were selected for further study and considered
204 free from obvious diagenetic alteration. Representative samples were selected from both
205 cores based on the X-ray images for SEM, thin-section and XRD analysis. Additional
206 samples were selected after geochemical analysis targeting intervals with unusually high
207 or low Sr/Ca ratios. The powder-XRD diffractometer at Rheinisch-Westfaelische
208 Technische Hochschule (RWTH) Aachen University was calibrated to detect and
209 quantify very low calcite contents above $\sim 0.2\%$ following the method of Smodej et al.

210 (2015). In addition, the 2D-XRD system Bruker D8 ADVANCE GADDS was used for
211 XRD point-measurements directly on the coral slab with a spatial resolution of ~ 4 mm
212 and a calcite detection limit of $\sim 0.2\%$ (Smodej et al., 2015). A 2-dimensional detector
213 allows the simultaneous data collection over a large 2θ range, which reduces the
214 counting time to 10 min for each sampling spot. The coral is mounted on a motorized
215 XYZ-stage and the position of each sample spot is controlled by an automated laser-video
216 alignment system. Multiple sample points can be predefined and measured automatically.
217 This method was used to test for the presence of secondary calcite along the sampling
218 traces of both corals.

219 Sr/Ca ratios were measured at the University of Kiel with a simultaneous
220 inductively coupled plasma optical emission spectrometer (ICP-OES, Spectro Ciros CCD
221 SOP; Zinke et al., 2014). Approximately 0.5mg of coral powder are dissolved in 1.00 ml
222 0.2M HNO₃. Prior to analysis, the solution is diluted with 0.2M HNO₃ to a final
223 concentration of ~ 8 ppm Ca. An analogue in-house coral powder standard (Mayotte) was
224 analyzed after every six samples. The international reference material JCp-1 (coral
225 powder) was analyzed with every sample batch. All calibration solutions are matrix-
226 matched to 8 ppm Ca. Strontium and Ca are measured at their 407 and 317 nm
227 emission lines. Our intensity ratio calibration strategy combines the techniques described
228 by de Villiers et al. (2002) and Schrag (1999). Analytical precision of Sr/Ca
229 determinations as estimated from replicate measurements of unknown samples is 0.15%
230 or 0.01 mmol/mol (1sigma).

231 The coral core chronologies were developed based on the seasonal cycle of Sr/Ca.
232 We assigned the coldest month (either August or September) to the highest measured

233 Sr/Ca ratio (Sr/Ca maxima) in any given year, according to both *in situ* SST and grid-SST
234 (Extended reconstructed SST; Smith et al., 2008). We then interpolated linearly between
235 these anchor points to obtain age assignments for all other Sr/Ca measurements. In a
236 second step, the Sr/Ca data were interpolated to 12 equidistant points per year to obtain
237 monthly time series using AnalySeries 2.0 (Paillard et al., 1996). This approach creates a
238 non-cumulative time scale error of 1 - 2 month in any given year, due to interannual
239 differences in the exact timing of peak SST. The monthly interpolated Sr/Ca time series
240 were cross-checked with the chronologies from coral XDS to reveal the timing of high
241 and low density banding. High density bands in both corals formed in summer (low
242 Sr/Ca) of any given year.

243

244 **4 Historical SST data**

245 Historical SST data collected primarily by ships-of-opportunity have been summarised
246 in the comprehensive ocean atmosphere data set (ICOADS) to produce monthly averages
247 on a 2x2° grid basis (Woodruff et al., 2005). In the grid that includes Rodrigues Island
248 the data are extremely sparse (Fig. A1). Since the uncertainty in SST bias adjustments
249 due to measurement errors is much larger for Southern Hemisphere than the Northern
250 Hemisphere (Jones, 2016) data, we therefore extracted a large number of SST and marine
251 air temperature datasets for our region in comparison to our coral proxy data. We
252 extracted SST from extended reconstructed SST (ERSST version 3b/version 4; Smith et
253 al., 2008), also based on ICOADS data, which uses sophisticated statistical methods to
254 reconstruct SST from sparse data. From ERSST, we extracted data in the 2x2° grid
255 centred at 61-63°E, 19-21°S (Table A1). Furthermore, we used Met Office Hadley

256 Centre's sea ice and sea surface temperature (HadISST) data for the grid 62-63°E, 19-
257 20°S (Rayner et al., 2003; Kennedy et al., 2011; Table A1). HadISST temperatures were
258 reconstructed using a two-stage reduced-space optimal interpolation procedure, followed
259 by superposition of quality-improved gridded observations onto the reconstructions to
260 restore local detail. Since January 1982, SST time series for HadISST use the optimal
261 interpolation SST (OISST; 1x1°), version 2 (Reynolds et al., 2002) that includes
262 continuous time series of satellite-based SST measurements. We also extracted Advanced
263 Very High Resolution Radiometer (AVHRR) SST at 0.25x0.25° resolution (Reynolds et
264 al., 2007) from 1985 to 2006 . SST from the 5x5° HadSST3, the most sophisticated bias-
265 corrected SST data to date, were downloaded for the region 60-65°E, 15-20°S (Kennedy
266 et al., 2011; Appendix Table 1) but contains data gaps throughout the record due to strict
267 quality control. SST is reported as anomalies relative to the 1961 to 1990 mean
268 climatology. In addition, we extracted 5x5° night-time marine air temperature data from
269 HadMAT1 and HadNMAT2 datasets (Kent et al., 2013). HadNMAT2 also contains data
270 gaps throughout the record due to strict quality control. Night-time marine surface air
271 temperature is highly correlated with SST but free of the biases introduced by changes in
272 SST measurement techniques (Tokinaga et al., 2012).

273

274 **5 Results**

275 **5.1 Coral Sr/Ca seasonality, variability and trends**

276 The average growth rate of the corals Totor (224 years) and Cabri (130 years)
277 were $9.82 \pm 0.19 \text{ mm y}^{-1}$ and $11.79 \pm 0.25 \text{ mm y}^{-1}$, respectively (Table 1; Fig. S1). The Cabri
278 core shows a growth disturbance at 1907 that led to partial colony mortality (see Suppl.

279 Information). This lower core section is overprinted by diagenesis and it is therefore not
280 suitable for climate studies or to determine density and calcification rates.

281 For the period of overlap (1945 to 2005) there is an offset in mean Sr/Ca of
282 0.0242 mmol/mol between the colonies. Both cores show a distinct seasonality in Sr/Ca
283 throughout their record length (Fig. 2a). The seasonality in the Totor core (0.283 ± 0.049
284 mmol/mol) is on average slightly higher compared to the Cabri core (0.238 ± 0.055
285 mmol/mol), yet the difference is not statistically significant (both overlap within 1σ). To
286 eliminate the offset between Sr/Ca time series we calculated Sr/Ca anomalies by
287 subtracting their mean relative to the 1961 to 1990 reference period (Figure 2a).

288 Between 1945 and 2006 both cores record higher Sr/Ca anomalies (a period of
289 cooling) that started in the mid 1950's and lasted until the early 1970's. Both cores show
290 a pronounced trend to more negative Sr/Ca values (warming) starting in the 1970's and
291 reduced seasonality in that period (Fig. 2a). After 1984 Sr/Ca in the Cabri core further
292 decreases (warms) while Sr/Ca in the Totor core records no trend. This highlights that the
293 long-term trend estimates after 1984 need to be viewed with caution.

294 The Sr/Ca time series in the Totor core extends to 1781 (Fig. 2a). Marked
295 negative Sr/Ca anomalies (warmer) are observed during the first half of the 20th century
296 centered at 1918/19, 1936-41 and in the period 1948-1951 that exceed anomalies in the
297 1961 to 1990 reference period. Sr/Ca anomalies between 1850 and 1890 are higher
298 (cooler) while decadal periods with lower (warmer) Sr/Ca are observed between 1781
299 and 1850 relative to 1961 to 1990.

300

301 **5.2 Diagenetic tests for alterations of Sr/Ca profiles**

302 Representative samples for diagenetic screening with XRD, SEM and light
303 microscopy were identified on the coral slabs using the X-radiographs. Additionally,
304 intervals with presumably anomalous proxy values (warm or cold anomalies) were
305 analyzed with the same methods. Ten thin-sections, six SEM samples, ten powder-XRD
306 and thirteen spot-2D-XRD samples were analyzed from coral core Totor (Fig. 3). For
307 coral core Cabri, seven thin-sections, one powder-XRD and six 2D-XRD samples were
308 analyzed. Neither powder nor spot-XRD analysis detected any calcite. Thin-section
309 analysis indicates a growth break within core section 12 of Totor that is also apparent in
310 the radiograph (Fig. 4; Appendix Fig. 5). Close to this break the coral is strongly affected
311 by bioerosion and encrustation by red algae (Fig. 3e). The sampling transect for
312 geochemical analysis, however, excluded this area and is therefore the reported data are
313 not affected by diagenesis (Fig. 8e). Combined SEM, EDS and XRD analysis shows low
314 amounts of patchy distributed isopachous ($\sim 2\mu\text{m}$) fibrous aragonite cement in Totor core
315 section 6 (1916-1921), 7 (1882-1887) and 11 (~ 1809).

316 Aragonite cement should lead to higher Sr/Ca values and lower reconstructed
317 temperatures (Hendy et al., 2007). An interesting outcome is that the observed diagenesis
318 is not able to explain changes in the Sr/Ca ratios except for the Totor core section 7. Here
319 the observed aragonite cement is associated with relatively high Sr/Ca values resulting in
320 an apparent cold anomaly. No anomalously high Sr/Ca ratios are associated with the
321 patchy aragonite cements in Totor core sections 6 and 11. Instead core sections 6 and 11
322 are characterized by low Sr/Ca ratios resulting in apparent relatively warm reconstructed
323 temperatures. All other samples from the core sections Totor 3, 4, 8, 9 and 10 are devoid
324 of diagenetic alteration. In summary, a diagenetic influence on the proxy record and

325 resulting SST reconstructions are only evident for Totor core section 7 (years 1882-
326 1887). Core Cabri showed only localized (single month) positive Sr/Ca anomalies (cool
327 SST bias; Fig. 3f). Thin-section and XRD analysis did not establish any diagenetic
328 alteration, but the coral locally contained aragonitic sediment partially filling pore spaces
329 (Fig. 3f). This aragonitic sediment potentially could have caused the isolated Sr/Ca peaks
330 (high Sr/Ca) in the record. These individual data points were omitted from further
331 analysis.

332

333 **5.3. Calibration of coral Sr/Ca-SST with in-situ and gridded SST**

334 The coral Sr/Ca from both cores was calibrated with *in situ* SST, ERSSTv.3b and
335 AVHRR SST for the period 2002 to 2006 using the minima and maxima in any given
336 year, as well as monthly values with AVHRR SST for 1981 to 2006 (Fig. 4; Tab. A2).
337 There is a relatively large variance in the Sr/Ca-SST relationships depending on the coral
338 core and the SST record. The slopes of the ordinary least squares regressions vary
339 between -0.0384 to -0.0638 mmol/mol per 1°C (Tab. A2). The lowest slopes are obtained
340 with *in situ* SST and the highest with ERSSTv.3b (Tab. A2). The range of this variance is
341 consistent with the results of Corrège (2006), who used a set of more than 30 coral Sr/Ca
342 records from various ocean basins and different coral genera. We reconstructed absolute
343 SST for the period of overlap with *in situ* SST from 2002 to 2006 from both coral cores
344 (Fig. 4). The Sr/Ca-SST in the Totor core shows the best fit with *in situ* SST in terms of
345 the seasonal amplitude. The Sr/Ca-SST in the Cabri core overestimates the winter SST of
346 2002 and 2005, yet agrees well for 2003 and 2004 (Fig. 4). Taking into account the
347 uncertainties (measurement error, regression error) in absolute SST from Sr/Ca for Cabri

348 and Totor of 1.23°C and 1.05°C (1σ), respectively, the coral data agree with *in situ* SST
349 within the 1σ uncertainty.

350

351 **5.4. Validation of Sr/Ca-SST anomalies with gridded SST products**

352 To eliminate errors associated with absolute SST reconstructions from coral Sr/Ca
353 we calculated relative changes in SST for the coral temperature records relative to the
354 1961 to 1990 mean based on the established empirical relationship of -0.0607 mmol/mol
355 per 1°C derived from >30 published Sr/Ca calibrations (Corrège, 2006; Nurhati et al.,
356 2011). This slope is well within the range of our regressions based on a variety of SST
357 datasets and consistent with the results of Corrège (2006). (Tab. A2). We consider the
358 mean Sr/Ca-SST slope of Corrège (2006) to be much more reliable than our short *in situ*
359 calibration. We use a conservative estimate of the uncertainty around relative SST
360 changes based on the difference between lower (-0.04) and upper slope (-0.084) estimates
361 from these regression equations, thus ± 0.02 mmol per 1°C or $\pm 0.33^\circ\text{C}$ (following Gagan
362 et al., 2012; Tab. A2).

363 We validated the coral derived annual mean SST reconstruction against local Air
364 Temperature (AT), ERSSTv3b, ERSST4, HadISST, HadSST3, HadMAT1 and
365 HadNMAT2 for the period 1951 to 2006 (Figure 5; See Supplementary Tables 1-16 for
366 mean annual correlations). The Cabri coral SST record records the highest correlations
367 with HadISST and HadMAT1 in the grid box surrounding Rodrigues Island while the
368 overall best fit is obtained with local Rodrigues AT. Core Totor has no significant
369 correlations with both ERSST products and HadISST, yet shows significant correlations
370 with HadSST3, HadMAT1 and HadNMAT2 (Suppl. Tabs. 11, 15, 16). Discrepancies

371 between AT and gridded SST products are observed between 1951 and 1955 with AT
372 indicating significantly warmer temperatures. Cabri tracks grid-SST between 1951 and
373 1955 while Totor shows warm anomalies similar to AT. Taking into account the
374 uncertainty of $\pm 0.33^{\circ}\text{C}$ based on the regression error, however, Cabri SST agrees with
375 gridded SST and AT within 1σ while Totor shows less agreement.

376 For the period 1951 to 2005, we used AT, ERSSTv3b, ERSST4, HadISST,
377 HadSST3, HadMAT1 and HadNMAT2 to validate trends in annual mean coral Sr/Ca-
378 SST anomalies (Fig. 5). The uncertainty for the trend estimates in coral Sr/Ca SST is
379 calculated from the square root of the sum of squares of the regression error and the error
380 in the slope of the Sr/Ca-SST relationship. The long-term trends in Sr/Ca-derived SST
381 anomalies for the period 1951 to 2005 for Cabri and Totor converted to SST, using the
382 published Sr/Ca-SST relationship of $-0.0607\text{mmol/mol per }1^{\circ}\text{C}$, indicate a warming of
383 $1.38\pm 0.39^{\circ}\text{C}$ and cooling of $-0.49\pm 0.41^{\circ}\text{C}$, respectively. Instrumental SST indicate a
384 warming trend of $0.61\pm 0.13^{\circ}\text{C}$ for HadISST, $0.72\pm 0.11^{\circ}\text{C}$ for ERSST3b ($0.86\pm 0.12^{\circ}\text{C}$
385 for ERSST4) and $0.78\pm 0.12^{\circ}\text{C}$ for HadSST3. Air Temperature at Rodrigues weather
386 station recorded a warming trend of $0.46\pm 0.17^{\circ}\text{C}$. All trends are statistically significant
387 at the 98% level with the exception of the negative trend in Sr/Ca SST anomalies in the
388 Totor core which is not significant.

389 For the pre-1945 period we used ERSSTv3b, HadISST, HadSST3 HadMAT1 and
390 HadNMAT2 to validate annual mean coral Sr/Ca-SST from core Totor (Fig. 2). We stress
391 that the number of SST observations in the ICOADS SST and marine AT database is
392 extremely sparse for our region (Fig. A1). In general, the Totor SST record is a valid
393 reconstruction for the region surrounding Rodrigues Island for several decades with the

394 possible exception of 1854-1860, 1916-1921, 1936-1941 and 1948-1951 (Fig. 2). The
395 Totor coral SST time series displays significantly higher SST anomalies compared to all
396 gridded SST reconstructions in the 1850's, between 1916-1921, 1936-1941 and 1948-
397 1951 and lower SST anomalies for brief periods between 1850 and 1890. Interestingly,
398 the Totor Sr/Ca-SST has significant correlations with HadSST3, HadMAT1 and
399 HadNMAT2 observational time series only (Suppl. Tabs. 11, 15, 16). The cool bias in
400 coral derived SST between 1882 and 1887 (core section 7) is related to diagenetic
401 alterations, but none of the anomalously warm periods can be explained by diagenesis
402 (see next section). We assessed the orientation of corallites relative to the coral slab
403 surface to test for sampling artifacts that might have altered our Sr/Ca data which we
404 summarized in Tables 2 and 3, illustrate in Figure 2 and discuss in section 6.1. Most
405 anomalous warm periods show sub-optimal orientation of sampling path with corallites at
406 an angle to the slab surface (see 6.1).

407

408 **5.5 Large scale teleconnections between 1945 and 2006**

409 The large-scale teleconnections with SST are significant for the Cabri Sr/Ca-SST
410 time series starting in 1945 (Figs. 7 and 8), while core Totor has statistically insignificant
411 correlations in that period. This indicates that the Cabri time series is more reliable for the
412 recent 60 years for monthly averages and annual means and shows the strongest
413 correlations across the Indo-Pacific (Figs. 7 and 8). Therefore, we assess the large-scale
414 climate teleconnections only for the period between 1945 and 2006.

415 The detrended Cabri Sr/Ca-SST records shows positive correlations for austral
416 summer and annual means with Indian Ocean wide SST, a positive correlation with the

417 central and eastern Pacific SST and negative correlations with North Pacific SST typical
418 for the spatial ENSO and PDO pattern (Figure 7; Supplementary Tables 17-19). The
419 detrended mean annual time scales (July-June) and austral summer (JFM) record for the
420 Cabri SST indicates a positive correlation with southern Indian Ocean SST along a
421 southeast to northwest band stretching along the trade wind belt (Figure 7d-f). The
422 correlation with the southern Indian Ocean trade wind belt remains stable over different
423 record length and is most pronounced post 1971. The detrended Cabri record shows
424 negative correlations ($r = -0.39$; $p < 0.001$; $N = 48$) with the SIOD index for austral summer
425 month. This agrees with similar sign and strength of correlations of HadISST for
426 Rodrigues with the SIOD ($r = -0.43$; $p < 0.001$; $N = 48$; Fig. A3; Tab. S19-21). We find
427 positive correlations with the eastern Pacific SST and negative correlations with the
428 northern Pacific along 40°N and stretching between 160°E and 150°W . The SST pattern
429 mimics part of the typical spatial ENSO and PDO pattern across the Indo-Pacific (Mantua
430 et al., 1997; McPhaden et al., 2006). Stratifying the correlations into negative and
431 positive PDO phases between 1950-1975 and 1976 to 1999 reveals the PDO-like spatial
432 SST pattern (Fig. 8).

433 Comparison with available coral proxy records from the wider trade wind belt
434 region in the SWIO between 12 to 21°S and 50 to 63°E reveals that the Cabri record
435 agrees best with the Sr/Ca-SST from St. Marie Island (core STM2 in Grove et al., 2013a;
436 $r = 0.25$; $N = 50$, $p = 0.08$) on mean annual time scales, yet not with the La Reunion record
437 (Fig. 9). Cabri shows the highest correlation of the three coral records from SWIO with
438 HadISST for the larger grid-box between 12 to 21°S and 50 to 63°E ($r = 0.49$, $p = 0.001$,

439 N=60) while both St. Marie and La Reunion corals show no statistically significant
440 correlations.

441

442 **6 Discussion**

443 **6.1 Diagenesis, coral growth pattern changes and potential biases in Sr/Ca derived** 444 **SST**

445 Generally diagenesis could be excluded as a major cause of discrepancies between
446 coral SST and grid-SST. For core Totor, only for the period between 1882 and 1887 is
447 diagenesis the cause of a cool bias on our coral SST reconstruction (Figure 3d). Core
448 Cabri showed only localized positive Sr/Ca anomalies (cool SST bias) caused by
449 aragonitic sediment trapped within growth framework pores (Fig. 3f). These specific
450 samples have been removed before interpolation. Having excluded diagenesis for almost
451 all of the record, we assessed sampling biases due to changes in the orientation of growth
452 axes and positioning of corallites to the slab surface (Tab. 2 & 3). De Long et al. (2012)
453 showed clear evidence for warm or cool biases in coral Sr/Ca-SST reconstructions caused
454 by suboptimal orientation of corallites in corals from New Caledonia. We have adopted a
455 similar approach to test for sampling biases in our two cores (summarized in Table 2 &
456 3). We found that core Totor contained areas where a sampling bias could explain
457 anomalous Sr/Ca-derived SST (1781-1797, 1825-1835, 1854-1860, 1916-1921, 1936-
458 1941 and 1948-1951, 1984-2001). We provide a detailed explanation of the potential
459 biases in core Totor and its co-variability with a tropical western Indian Ocean coral SST
460 reconstruction from the Seychelles pre-1900 (Pfeiffer and Dullo, 2006; Fig. S2) in the
461 Supplementary Information that is of particular importance for coral paleoclimatologists.

462 De Long et al. (2012) showed that warm biases were often caused by corallites
463 orientated at an angle to the slab surface and where growth orientation had changed.
464 Sampling of these suboptimal intervals will have seasonal cycles with more summer
465 Sr/Ca values than winter values causing an apparent warm bias. Such a relationship could
466 not be identified for core Totor, for instance for the largest single warm anomaly in the
467 years 1916 to 1921. Nevertheless, the extreme warm anomaly between 1916 to 1921
468 could be associated with an unidentified vital effect (Alpert et al., 2015). Interestingly,
469 despite the potential influence of vital effects on the trend, the seasonality in this core
470 section was well preserved. This implies that seasonality can be captured robustly while
471 absolute values and trends are potentially biased by vital effects. This adds confidence for
472 the study of seasonality from fossil corals where vital effects are harder to distinguish
473 from true variability due to the lack of SST data for verification.

474 For the core tops between 1984 and 2005, Sr/Ca trends in cores Totor and Cabri
475 deviate with Totor showing a statistically insignificant cooling trend while Cabri shows a
476 strong warming trend (Fig. 2). Our analysis of polyp growth revealed a change in growth
477 pattern near the top of core Totor: the corallites form parallel, elongated rods of septa for
478 the entire period 1984 to 2005 (Fig. 6). Cabri shows a normal growth pattern, with an
479 optimal orientation of corallites at the core top between 1984 and 2006 (Fig. A5), with
480 the exception of sub-optimal corallites in the period 2000 to 2006. The core top of the
481 Totor coral skeleton has very low overall density. The Sr/Ca ratios show an increased
482 seasonality, with colder winter values compared to core Cabri, while summer values are
483 not affected. At first glance, the peculiar structure of the corallites in Totor would suggest
484 optimal vertical growth of the corallites with the polyps clearly visible from the apex of

485 the core slab. This structure is, however, clearly associated with high Sr/Ca ratios and
486 artificially cold SST anomalies. A similar growth pattern was found in a *Porites lutea*
487 from St. Marie Island off East Madagascar (core STM4 in Grove et al. 2013a). Grove et
488 al. (2013a) ascribed the Sr/Ca trend difference between cores STM2 and STM4 to
489 changes in coral growth and calcification, yet their results were not conclusive. Re-
490 examination of core STM4 revealed that it also forms the parallel-elongated rods of septa
491 in the core top, which was biased towards high Sr/Ca ratios and therefore cold SST
492 anomalies. STM4 also showed low densities in this core top section that agrees with low
493 density in Totor. Inspection of various core sections in Totor and other coral cores
494 revealed that similar elongated rods of septa (not sampled down core) are formed
495 between neighboring growth fans of septa. We propose that these parallel septa grow
496 very fast in summer and winter, therefore show weak density contrast with overall low
497 skeletal density. Similar anomalously high Sr/Ca values between adjacent fans of
498 corallites were reported for Great Barrier Reef corals (see Figure 4 in Alibert and
499 McCulloch, 1997). Alibert and McCulloch (1997) suggested that less optimal growth
500 conditions may result in smaller corallites and overall low skeletal density affecting
501 Sr/Ca ratios. We suggest that core tops from *Porites* sp. with similar parallel septa should
502 be avoided for sampling since it can cause a cold bias in Sr/Ca-based SST
503 reconstructions.

504 Overall, our test for sampling biases to a large extent confirms the findings of De
505 Long et al. (2012) and indicates that such analysis should accompany climate
506 reconstructions from coral cores. Our results suggest that a new core needs to be obtained
507 from the Totor colony or other large *Porites* sp. in order to overcome the SST biases

508 identified in the current record. The Cabri coral (>3.5m in height) would be an ideal site
509 since it provided an excellent and largely un-biased record of SST for the period 1945 to
510 2006. The 1907 dead surface was present, however, in three long cores drilled from the
511 Cabri coral at different angles, which could undermine the SST reconstruction for a few
512 decades below the mortality event. The reason for the mortality event could not be
513 determined.

514

515 **6.2 Trends and large-scale climate teleconnections since 1945 from core Cabri**

516 Based on our analysis of corallite orientations and diagenesis, we conclude that
517 core Cabri provides a largely un-biased record to assess SST trends and interannual
518 variability since 1945. The Cabri time series recorded a higher SST rise ($1.38\pm 0.41^{\circ}\text{C}$)
519 than instrumental data between 1945 and 2006, which ranged between 0.61 to
520 $0.86\pm 0.15^{\circ}\text{C}$. The trend in Cabri agrees with all SST datasets within 2σ , whereby the
521 lower range of uncertainty for the Cabri trend estimates ($\sim 1^{\circ}\text{C}$) is in close agreements to
522 trends from gridded SST datasets. Most of the accelerated warming trend in Cabri
523 resulted from the recent 6 years where the orientation of the corallites was sub-optimal.
524 We conclude that the SST trend in Cabri closely follows open ocean grid-SST which both
525 indicate strong warming ($\sim 0.68\text{--}1^{\circ}\text{C}$) of the south-central Indian Ocean over the past 60
526 years. Roxy et al. (2014) reported that during 1901–2012, the Indian Ocean warm pool
527 warmed by 0.78°C while the western Indian Ocean ($5^{\circ}\text{S}\text{--}10^{\circ}\text{N}$, $50^{\circ}\text{--}65^{\circ}\text{E}$) experienced
528 anomalous warming of 1.28°C in summer SSTs. Our results for Cabri are therefore not
529 unusual and within the range of observed Indian Ocean SST trends (Annamalei et al.,
530 2005; Alory et al., 2007; Koll Roxy et al., 2014). The strong warming in the southern

531 Indian Ocean trade wind belt could potentially alter the monsoon circulation, especially
532 during the monsoon onset phase in austral autumn (March to May; Annamalei et al.,
533 2005). Both, our Cabri coral SST time series and SST products indicate the strongest
534 warming for the March to May season (not shown). Rodrigues station precipitation is
535 strongly positively correlated with SST between March and May. When precipitation is
536 anchored over a warmer SWIO between March and May it can prevent the movements of
537 the ITCZ towards the North and potentially disrupt the Asian monsoon onset (Annamalei
538 et al., 2005).

539 The Cabri record also indicated that Rodrigues Island has negative correlations
540 with the SIOD. Rodrigues Island is located at the westernmost edge of the northeastern
541 flank of the SIOD that stretches from the south-central western Indian Ocean to the coast
542 of Western Australia. There is no other coral reef between Rodrigues Island and the West
543 Australian coast that is able to track the SIOD. Rodrigues is therefore the only coral reef
544 at which SST variability tracks the SIOD at its northeastern flank. The Ifaty corals off
545 southwest Madagascar was shown to track the southwestern flank of the SIOD (Zinke et
546 al., 2004). Our results suggest that a combination of corals off southwest Madagascar
547 with longer records from Rodrigues could provide valuable records of past SIOD
548 variability.

549 The Cabri coral SST reconstructions revealed a clear ENSO/PDO teleconnection
550 pattern for mean annual and austral summer averages with positive correlations across the
551 Indian Ocean in response to ENSO and PDO (Xie et al., 2016; Fig. 7 and 8; Suppl. Tabs.
552 17-19). The ENSO/PDO teleconnection was stable for the recent 60 years, yet appears
553 strongest between 1971 and 2006 (Fig. 7c,f). The latter period is known for increased

554 occurrence of El Niño events and a switch to a positive PDO phase up to 1999
555 (McPhaden et al., 2006). These results are in agreement with ENSO/PDO pattern
556 correlations observed in other coral records from the southwestern Indian Ocean (Pfeiffer
557 et al., 2004; Crüger et al., 2009). This is the first Indian Ocean coral SST reconstruction,
558 however, that shows a clear Indian Ocean SST relationship with the PDO. Previous
559 studies have shown only indirect links between the PDO with southwestern Indian Ocean
560 sea level pressure and salinity (Crueger et al., 2009), hydrological balance (Zinke et al.,
561 2008) and river runoff (Grove et al., 2013b). In addition, our record is the first Sr/Ca
562 record for the south-central Indian Ocean, which is currently the most reliable proxy for
563 SST in corals. The only long record from this region of the Indian Ocean is a stable
564 isotope record from La Reunion Island that mainly records salinity variations (Pfeiffer et
565 al., 2004). The lack of correlation between the La Reunion and Cabri record is therefore
566 not surprising and points to the need to develop Sr/Ca time series for La Reunion (Fig. 9).
567 The St. Marie Island Sr/Ca coral record shows reasonable agreement with Cabri, with the
568 SST shift in the 1970's especially apparent in both records (Fig. 9). The St. Marie Island
569 record is, however, not well suited to track the wider trade wind belt variations.
570 Therefore, our new proxy record from Rodrigues for the period between 1945 and 2006 is
571 a valuable addition to the sparse Indian Ocean coral proxy network. It also establishes
572 that records from Rodrigues are well suited to study decadal climate teleconnections with
573 the (extra)tropical Pacific and the wider Indian Ocean.

574

575 **7 Acknowledgements**

576 The coral paleoclimate work was supported as part of the SINDOCOM grant
577 under the Dutch NWO program ‘Climate Variability’, grant 854.00034/035. Additional
578 support comes from the NWO ALW project CLIMATCH, grant 820.01.009, and the
579 Western Indian Ocean Marine Science Association through the Marine Science for
580 Management program under grant MASMA/CC/2010/02. We thank the team of
581 SHOALS Rodrigues for their excellent support in fieldwork logistics and in the
582 organization of the research and CITES permits. We would also like to thank the
583 Rodrigues Assembly and the Mauritius Ministry for Fisheries for granting the research
584 and CITES permits. A Senior Curtin Fellowship in Western Australia, and an Honorary
585 Fellowship with the University of the Witwatersrand, South Africa, supported JZ. Bouke
586 Lacet and Wynanda Koot (VUA) helped cut the core slabs and prepared the thin sections.
587 Janice Lough and Eric Matson (AIMS) provided skilled technical support for coral core
588 densitometry measurements and data processing. We thank Dieter Garbe-Schönberg for
589 assistance with the ICP-OES measurements.

590

591 **References**

592 Alibert, C. and McCulloch M. T.: Strontium/calcium ratios in modern Porites corals from the
593 Great Barrier Reef as a proxy for sea surface temperature: calibration of the thermometer and
594 monitoring of ENSO, *Paleoceanography*, 12(3), 345-363, 1997.

595

596 Alory, G. and Meyers, G.: Warming of the Upper Equatorial Indian Ocean and Changes in the
597 Heat Budget (1960–99), *J. Climate*, 22, 93–113, 2009.

598

599 Alpert, A. E., Cohen, A. L., Oppo, D. W., DeCarlo, T. M., Gove, J. M., Young, C. W.
600 Comparison of equatorial Pacific sea surface temperature variability and trends with Sr/Ca
601 records from multiple corals. *Paleoceanography*, 31, 252-262, 2016.

602 Annamalai, H., Liu, P. and Xie, S.-P.: Southwest Indian Ocean SST Variability: Its Local
603 Effect and Remote Influence on Asian Monsoons, *Journal of Climate*, 18, 4150-4167, 2005.

604 Behera, S.K. and Yamagata, T. Subtropical SST dipole events in the southern Indian
605 Ocean, *Geophys. Res. Lett.* 28 (2), 327– 330, 2001.

606

607 Behera SK, Yamagata T. A dipole mode in the tropical Indian Ocean. *Geophysical Research*
608 *Letters*, 28, 327–330, 2001.

609

610 Carricart-Ganivet, J. P. and Barnes D. J.: Densitometry from digitized images of X-
611 radiographs: methodology for measurement of coral skeletal density, *Journal of Experimental*
612 *Marine Biology and Ecology*, 344, 67-72, 2007.

613

614 Charles, C. D., Hunter, D. E. and Fairbanks R. G.: Interaction between the ENSO and the Asian
615 Monsoon in a coral record of tropical climate, *Science*, 277, 925-928, 1997.

616

617 Cobb, K. M., Charles, C. D. and Hunter D. E.: A central tropical pacific coral demonstrates
618 pacific, Indian, and Atlantic decadal climate connections, *Geophysical Research Letters* 28(11),
619 2209-2212, 2001.

620

621 Cole, J. E., Dunbar, R. B., McClanahan, T. R. and Muthiga N. A.: Tropical Pacific forcing of
622 decadal SST variability in the Western Indian Ocean over the past two centuries. *Science* 287,
623 617-619, 2000.

624

625 Corrège, T., Sea surface temperature and salinity reconstruction from coral geochemical
626 tracers. *Palaeoeco. Palaeoclim. Palaeoeco.*, 232, 408-428, 2006.

627

628 Crueger, T., Zinke, J. and Pfeiffer M.: Patterns of Pacific decadal variability recorded by Indian
629 Ocean corals. *International Journal of Earth Sciences* 98, doi:10.007/s00531-00008-00324-
630 00531, 2009.

631

632 Deser, C., Phillips, A. S., and Hurrell, J. W.: Pacific Interdecadal climate variability:

633 linkages between the tropics and the North Pacific during boreal winter since 1900, J.
634 *Climate*, 17, 3109-3124, 2004.

635

636 DeLong, K. L., Quinn, T. M., Taylor, F. W., Shen, C.-C. and Lin, K.: Improving coral-base
637 paleoclimate reconstructions by replicating 350 years of coral Sr/Ca variations,
638 *Palaeogeography, Palaeoclimatology, Palaeoecology*, 373, 6-24, 2012.

639

640 DeVilliers, S., Sheng, G.T., Nelson, B.K.: The Sr /Ca-temperature relationship in coralline
641 aragonite: Influence of variability in (Sr/Ca)seawater and skeletal growth parameters,
642 *Geochimica et Cosmochimica Acta*, 58, 197-208, 1994.

643

644 Felis, T. and Paetzold, J.: Climate records from corals, In: *Marine Science Frontiers for*
645 *Europe*. Eds.: G. Wefer, F. Lamy and F. Mantoura. Berlin, Heidelberg, New York, Tokyo,
646 Springer, p. 11-27, 2003.

647

648 Funk, C., Dettinger, M. D., Michaelsen, J. C., Verdin, J. P., Brown, M. E., Barlow, M. and
649 Hoell, A.: Warming of the Indian Ocean threatens eastern and southern African food security
650 but could be mitigated by agricultural development, *Proceedings Nat. Acad. Sci.*, 105(32),
651 11081-11086, 2008.

652

653 Gagan, M. K., Dunbar, G. B. and Suzuki, A.: The effect of skeletal mass accumulation in
654 *Porites* on coral Sr/Ca and d18O paleothermometry, *Paleoceanography* 27, PA1203,
655 doi:10.1029/2011PA002215, 2012.

656

657

658 Grove, C. A., Kasper, S., Zinke, J., Pfeiffer, M., Garbe-Schönberg, D. and Brummer, G.-J. A.:
659 Confounding effects of coral growth and high SST variability on skeletal Sr/Ca: Implications
660 for coral paleothermometry, *Geochem., Geophys. Geosyst.*, 14, doi:10.1002/ggge.20095,
661 2013a.

662

663 Grove, C. A., Zinke, J., Peeters, F., Park, W., Scheufen, T., Kasper, S.,
664 Randriamanantsoa, B., McCulloch, M. T. and Brummer, G.J.A. Madagascar corals reveal
665 multidecadal modulation of rainfall since 1708. *Climate of the Past* 9, 641-656, 2013b.
666

667 Hardman, E. R., Meunier, M. S., Turner, J. R., Lynch, T. L., Taylor, M. and Klaus R.: The
668 extent of coral bleaching in Rodrigues, *Journal of Natural History*, 38, 3077-3089, 2004.
669

670 Hardman, E. R., Stampfli, N. S., Hunt, L., Perrine, S., Perry, A. and Raffin, J. S.: The Impacts
671 of coral bleaching in Rodrigues, Western Indian Ocean, *Atoll Research Bulletin*, 555, DOI:
672 10.5479/si.00775630.555.1, 2008.
673

674 Helmle, K. P., Dodge, R.E., Swart, P.K., Gledhill, D.K. and Eakin, C.M.: Growth rates of
675 Florida corals from 1937 to 1996 and their response to climate change, *Nat. Commun*, 2, 215
676 doi: 10.1038/ncomms1222, 2011.
677

678 Hendy, E. J., Gagan, M. K., Lough, J. M., McCulloch, M., and deMenocal P. B.: Impact of
679 skeletal dissolution and secondary aragonite on trace element and isotopic climate proxies in
680 *Porites* corals, *Paleoceanography*, 22, PA4101, doi:10.1029/2007PA001462, 2007.
681

682 Hoell, A., Funk, C., Zinke, J., Harrison, L. Modulation of the Southern Africa precipitation
683 response to the El Niño Southern Oscillation by the subtropical Indian Ocean Dipole. *Climate*
684 *Dynamics*, DOI:10.1007/s00382-00016-03220-00386, 2016.
685

686 Jones, P. The Reliability of Global and Hemispheric Surface Temperature Records. *Advances in*
687 *Atmospheric Sciences*, 33, 269-282, 2016.
688

689 Kaplan, A. *et al.* Analyses of global sea surface temperature 1856-1991, *J. Geophys. Res.*, 103,
690 18567-18589, 1998.
691

692 Kennedy J.J., Rayner, N.A., Smith, R.O., Saunby, M. and Parker, D.E.: Reassessing biases and
693 other uncertainties in sea-surface temperature observations since 1850 part 1: measurement and

694 sampling errors, *J. Geophys. Res.*, 116, D14103, doi:10.1029/2010JD015218, 2011.
695

696 Kent, E.C., Rayner N.A., Berry D.I., Saunby M., Moat B.I., Kennedy J.J., Parker D.E.: Global
697 analysis of night marine air temperature and its uncertainty since 1880: the HadNMAT2
698 Dataset, *Journal of Geophys. Res.*, doi: 10.1002/jgrd.50152, 2013.
699

700 Koll Roxy, M., Ritika, K., Terray, P., Masson, S.: The curious case of Indian Ocean warming,
701 *Journal of Climate* 27, 8501-8509, 2014.
702

703 Krishnan, P., and Sugi, M.: Pacific decadal Oscillation and variability of the Indian
704 summer monsoon rainfall, *Climate Dynamics*, 21, 233-242, 2003.
705

706 Lee, S.-K., Park, W., Baringer, M. O., Gordon, A. L., Huber, B. and Liu ,Y.: Pacific origin of
707 the abrupt increase in Indian Ocean heat content during the warming hiatus, *Nature Geoscience*,
708 8, 445-449, 2015.
709

710 Lynch T.L., Meunier, M.S., Hooper, T.E.J., Blais, F.E.I., Raffin, J.S.J, Perrine, S., Félicité, N.,
711 Lisette, J., Grandcourt, J.W.: Annual report of benthos, reef fish and invertebrate surveys for
712 Rodrigues 2002, Shoals Rodrigues report, 30pp, 2002.
713

714 Mantua, N. J., Hare, S. R., Zhang, Y., Wallace, J. M., and Francis, R. C.: A Pacific decadal
715 climate oscillation with impacts on salmon, *Bull. Amer. Meteor. Soc.*, 78, 1069–1079, 1997.
716

717 Mart, Y.: The tectonic setting of the Seychelles, Mascarene and Amirante plateaus in the
718 Western Equatorial Indian ocean, *Marine Geology*, 79, 261-274, 1988.
719

720 McGregor H. V. and Gagan M. K.: Diagenesis and geochemistry of *Porites* corals from Papua
721 New Guinea: implications for paleoclimate reconstruction, *Geochim. Cosmochim. Acta*, 67,
722 2147–2156, 2003.
723

724 McGregor, H. V. and Abram, N. J.: Images of diagenetic textures in Porites corals from Papua
725 New Guinea and Indonesia, *Geochemistry, Geophysics, Geosystems* 9(10),
726 doi:10.1029/2008GC002093, 2008.
727

728 McPhaden, M. J., Zebiak, S. E., Glantz, M. H.: ENSO as an Integrating Concept in Earth
729 Science, *Science*, 314, 1740-1745, 2006.
730

731 Meehl, G. A., and Hu, A.: Megadroughts in the Indian Monsoon Region and Southwest North
732 America and a mechanism for associated Multidecadal Pacific Sea Surface Temperature
733 Anomalies, *J. Climate*, 19, 1605-1623, 2006.
734

735 Nakamura, N., Kayanne, H., Iijima, H., McClanahan, T. R., Behera, S. K. and Yamagata, T.:
736 Mode shift in the Indian Ocean climate under global warming stress, *Geophysical Research*
737 *Letters*, 36, L23708, doi:10.1029/2009GL040590, 2009.
738

739 New A. L., Alderson S. G., Smeed D.A., Stansfield K.L.: On the circulation of water masses
740 across the Mascarene Plateau in the South Indian Ocean, *Deep-Sea Research I* 54, 42–74, 2007.
741

742 New A. L., Stansfield, K., Smythe-Wright, D., Smeed D. A., Evans, A. J. and Alderson, S. G.:
743 Physical and biochemical aspects of the flow across the, Mascarene Plateau in the Indian
744 Ocean, *Philosophical Transactions of the Royal Academic Society* 363, 151–168, 2005.
745

746 Nurhati, I. S., Cobb, K. M. and Lorenzo E. D. Decadal-Scale SST and Salinity Variations in the
747 Central Tropical Pacific: Signatures of Natural and Anthropogenic Climate Change. *Journal of*
748 *Climate* 24: 3294-3308, 2011.
749

750 Paillard, D., Labeyrie, L., Yiou, P.: Macintosh program performs time series analysis. *Eos*
751 *Trans AGU* 77, 379, 1996.
752

753 Pfeiffer, M., Timm, O. and Dullo, W.-C.: Oceanic forcing of interannual and multidecadal

754 climate variability in the southwestern Indian Ocean: Evidence from a 160 year coral isotopic
755 record (La Reunion, 50E, 21S). *Paleoceanography*, 19, PA4006, doi:10.1029/2003PA000964,
756 2004.

757

758 Pfeiffer M. and Dullo, W.-Ch. Monsoon-induced cooling of the western equatorial Indian
759 Ocean as recorded in coral oxygen isotopes records from the Seychelles covering the period
760 1840-1994 AD. *Quat Sci Rev* 25:993–1009, 2006.

761

762 Pfeiffer, M., Dullo, W.-C., Zinke, J. and Garbe-Schoenberg, D.: Three monthly coral Sr/Ca
763 records from the Chagos Archipelago covering the period of 1950-1995 A.D.: reproducibility
764 and implications for quantitative reconstructions of sea surface temperature variations,
765 *International Journal of Earth Sciences*, 98, doi:10.007/s00531-00008-00326-z, 2009.

766

767 Rayner, N. A., Parker, D. E., Horton, E. B., Folland, C. K., Alexander, L. V., Rowell, D. P.,
768 Kent, E. C. and Kaplan A.: Global analyses of sea surface temperature, sea ice, and night
769 marine air temperature since the late nineteenth century. *Journal of Geophysical Research*
770 108(D14), doi:10.1029/2002JD002670, 2003.

771

772 Reason, C.J.C. Subtropical Indian Ocean SST dipole events and southern African rainfall,
773 *Geophys. Res. Lett.*, 28 (11) 2225–2227, 2001.

774

775 Reynolds, R.W., Rayner, N.A., Smith, T.M., Stokes, D.C., Wang W.: An improved in situ and
776 satellite SST analysis for climate, *Journal of Climate*, 15, 1609–1625, 2002.

777

778 Reynolds, R. W., Smith, T. M., Liu, C., Chelton, D. B., Casey, K. S. and Schlax, M. G.: Daily
779 high-resolution blended analyses for sea surface temperature, *J. of Climate*, 20, 5473-5496,
780 2007.

781

782 Sayani, H. R., Cobb, K. M., Cohen, A. L., Crawford Elliott, W., Nurhati, I. S., Dunbar, R. B.,

783 Rose, K. A., Zaunbrecher, L. K.: Effects of diagenesis on paleoclimate reconstructions from
784 modern and young fossil corals, *Geochimica et Cosmochimica Acta*, 75, 6361–6373, 2011.
785

786 Schott, F.A., McCreary, J.P.: The monsoon circulation of the Indian Ocean, *Progress in*
787 *Oceanography*, 51, 1–123, 2001.
788

789 Schrag, D.P.: Rapid analyses of high-precision Sr/Ca ratios in corals and other marine
790 carbonates, *Paleoceanography*, 14, 2, 97-102, 1999.
791

792 Sheppard, C.R.C. Predicted recurrences of mass coral mortality in the Indian Ocean.
793 *Nature*, 425, 294-297, 2003.
794

795 Smith, T.M., Reynolds, R.W., Peterson, T.C., Lawrimore, J.: Improvements to NOAA’s
796 historical merged land–ocean surface temperature analysis (1880–2006), *J. of Climate*, 21,
797 2283, 2008.
798

799 Smodej, J., Reuning, L., Wollenberg, U., Zinke, J., Pfeiffer, M. and Kukla, P. A.: Two-
800 dimensional X-ray diffraction as a tool for the rapid, nondestructive detection of low calcite
801 quantities in aragonitic corals, *Geochemistry, Geophysics, Geosystems*, 16,
802 10.1002/2015GC006009, 2015.
803

804 Tokinaga, H., Xie, S.P., Deser, C., Kosaka, Y., Okumura, Y. M.: Slowdown of the
805 Walker circulation driven by tropical Indo-Pacific warming. *Nature*, 491, 439-444, 2012.
806

807 Turner, J. and Klaus, R.: Coral reefs of the Mascarenes, Western Indian Ocean, *Philosophical*
808 *transactions of the Royal Academic Society*, 363, 229–250, 2005.
809

810 van Oldenborgh, G. J., Burgers, G.: Searching for decadal variations in ENSO
811 precipitation teleconnections, *Geophys. Res. Lett.*, 32, L15701, 2005.
812

813 Woodruff, S.D. *et al.*: ICOADS Release 2.5: Extensions and enhancements to the surface
814 marine meteorological archive, *Int. J. Climatol.*, 31, 951-967, 2011.
815

816 Xie, S.-P., Kosaka Y., Du Y., Hu K. M., Chowdary J. S., and Huang G.: Indo-western Pacific
817 ocean capacitor and coherent climate anomalies in post-ENSO summer: A review, *Adv. Atmos.*
818 *Sci.*, 33(4), 411–432, 2016.
819

820 Zinke, J., Pfeiffer, M., Park, W., Schneider, B., Reuning, L., Dullo, W.-Chr., Camoin, G. F.,
821 Mangini, A., Schroeder-Ritzrau, A., Garbe-Schönberg, D. and Davies, G. R.: Seychelles coral
822 record of changes in sea surface temperature bimodality in the western Indian Ocean from the
823 Mid-Holocene to the present, *Climate Dynamics*, 43 (3), 689-708, 2014.
824

825 Zinke, J., Pfeiffer, M., Timm, O., Dullo, W.-Chr. and Brummer, G. J. A. Western Indian
826 Ocean marine and terrestrial records of climate variability: a review and new concepts on
827 land-ocean interaction since A.D. 1660. *International Journal of Earth Sciences* 98,
828 Special Volume. doi:10.007/s00531-008-0365-5, 2009.
829

830 Zinke, J., Timm, O., Pfeiffer, M., Dullo, W.-Chr., Kroon, D. and Thomassin, B. A.
831 Mayotte coral reveals hydrological changes in the western Indian between 1865 to 1994.
832 *Geophysical Research Letters* 35, L23707, doi:10.1029/2008GL035634, 2008.
833

834 Zinke, J., Dullo, W.-Chr., Heiss, G. A. & Eisenhauer, A. ENSO and subtropical dipole
835 variability is recorded in a coral record off southwest Madagascar for the period 1659 to
836 1995. *Earth and Planetary Science Letters* 228 (1-2), 177-197, 2004.
837
838
839
840
841

842 **Tables**

Core name	GPS position	Species	Water depth (m)	Mean growth rate mm year⁻¹	Mean density g/cm³	Mean Calcification rate g/cm² year⁻¹
Totor	S19°40.237; E63°25.754	<i>Porites</i> <i>sp.</i>	4.0	9.2 (±0.19)	1.128 (±0.11)	1.07 (±0.18)
Cabri	S19°40.030, E63°26.065	<i>Porites</i> <i>lobata</i>	3.0	11.8 (±0.25)	1.36 (±0.12)	1.60 (±0.16)

843 Table 1 - Coral cores with their GPS co-ordinates and colony depths at low tide, with
 844 mean rates of extension, densities and calcification over the complete length of the
 845 individual records (1907 to 2006 for Cabri; 1781 to 2005 for Totor).

846

847

848

849

850

851

852

853

854

855

856

857

858

859

860

Section	Year	Orientation	Bias	Notes
1	2005-1987	Sub-optimal	cool	Corallites parallel to surface, yet straight angle; probably like a valley
2	1987-1982	Sub-optimal	cool	Corallites parallel to surface, yet straight angle; probably like a valley
2	1981-1977	Sub-optimal	none	Corallites at an angle to the surface; no bias
3	1978-1975	Sub-optimal	none	Corallites at an angle to the surface; no bias
3	1974-1958	Optimal	none	Corallites parallel to surface; no bias
4A	1958-1952	Sub-optimal	warm	Corallites at an angle to the surface; scallop texture from angles of corallites
4A	1951-1945	Sub-optimal	warm	Corallites at an angle to the surface; 1947-1952 low growth rate; reduced seasonality
4B	1947-1936	Optimal	none	Corallites parallel to surface, 1945-1947 better orientation than in slab 4A
4B	1938-1933	Sub-optimal	none	Corallites at an angle to the surface; 1936-1941 warm anomaly years show normal seasonality and high growth rate
5	1933-1922	Optimal	none	Corallites parallel to surface; 1922-1928 reduced seasonality
6	1921-1915	Sub-optimal	warm	1915-21 warm spikes shows slightly oblong corallites, yet normal seasonality; switch from optimal to sub-optimal orientation
6	1915-1896	Optimal to Sub-optimal	none	Corallites mostly parallel to surface, small section with corallites at slight angle;;
7	1897-1890	Optimal	none	Corallites parallel to surface
7	1887-1882	Optimal	cool	Diagenesis detected between years 1882-1887
7	1881-1872	Sub-optimal	none	Corallites at an angle to the surface; 1872 close to bioerosion track; 1878-1880 low seasonality, yet no effect
8	1872-1868	Sub-optimal	cool	Corallites at an angle to the surface; some corallites at almost 90° angle; 1868-1872 below bioerosion track; 1867-1871 low seasonality
9	1860-1854	Sub-optimal	warm	Corallites at an angle to the surface; 1854-1858 low seasonality, less winter samples
9	1856-1845	Sub-optimal	warm	Corallites parallel to surface; low seasonality with relatively warm winter samples
9	1844-1831	Optimal	none	Corallites parallel to surface; only 1831-1832 corallites at an angle to surface
10	1830-1827	Sub-optimal	warm	Corallites at an angle to the surface; oblong orientation
10	1826-1823	Disorganised	warm	Corallites rotating at 90° angle; low growth rate, seasonality reduced 1823-1825 with relatively warm winter samples
10	1822-1815	Optimal	none	Corallites parallel to surface; low growth rate; reduced seasonality 1818-1822, yet no effect on SST anomalies
11	1816-1806	Sub-optimal	none	Corallites at an angle to the surface, yet no effect on SST anomalies
11	1807-1798	Sub-optimal	none	Corallites at an angle to the surface in sub-optimal parts; Corallites rotating at 90° angle near terminating fans (not sampled); 3 growth axes with terminating fans in between (not sampled); 1799-1807 regular seasonality
11	1797-1792	Sub-optimal	warm	Corallites at an angle to the surface
12	1795-1792	Disorganised	warm	Corallites rotating at 90° angle; 1792-1791 long year, more summer samples
12	1791-1784	Sub-optimal	warm	Corallites parallel to surface; 1784-1787 Corallites at an angle to the surface; 1789-1794 seasonality distorted
12	1781-1783	Disorganised	warm	Corallites rotating at 90° angle; seasonality slightly distorted, apparently more summer samples

861 Table 2 – Summary of sampling issues detected in core Totor. Unbiased sampling tracks
862 indicated in bold.

Section	Year	Orientation	Bias	Notes
1	2007-2000	Sub-optimal	warm	Corallites parallel to surface; yet no clear growth fans
1	1999-1992	Optimal	none	Corallites parallel to surface
2	1984-1992	Sub-optimal	none	Corallites at an angle to the surface; oblong corallites
3	1983-1968	Sub-optimal	none	Corallites parallel to surface; yet no clear growth fan
4	1967-1964	Sub-optimal	none	Corallites at an angle to the surface
5	1963-1958	Optimal	none	Corallites parallel to surface
5	1957-1954	Sub-optimal	none	Corallites at an angle to the surface
5	1953-1945	Optimal	none	Corallites parallel to surface

863

864 Table 3 – Summary of sampling issues detected in core Cabri. Unbiased sampling tracks

865 indicated in bold.

866

867 **Figure captions**

868 Figure 1 – a) Map of Rodrigues Island with the position of the two corals cores at Totor

869 and Cabri indicated. The star shows the position of the CTD that collects SST and salinity

870 data. Polygon indicates the location of the Meteorological Station which records air

871 temperature, sunshine hours, wind speed and rainfall. b) Spatial correlation between

872 January-March averaged SIOD index (Behera and Yamagata, 2001) with HadISST for

873 Rodrigues Island (Rayner et al., 2003). c) Spatial correlation between July-June mean

874 annual averaged PDO index (Mantua et al., 1997) with HadISST (Rayner et al., 2003).

875 All correlations with detrended data. Only correlation with $p < 0.05$ are coloured.

876 Computed at KNMI climate explorer (van Oldenborgh and Burgers, 2005). Yellow star in

877 b) and c) marks the location of Rodrigues Island.

878

879 Figure 2 – a) Time series of monthly (thin solid lines) Sr/Ca anomalies (right Y-axis

880 converted) relative to the 1961 to 1990 climatological mean for coral cores Cabri (top),

881 Totor (middle) for the period 1781 to 2006. Annual mean time series of individual cores

882 (red line) b) Cabri and c) Totor compared to SST reconstructions: ERSSTv3b, ERSSTv4,

883 HadISST, HadSST3, HadMAT1 and HadNMAT2. See legend in b) and c) for colour

884 code. For all time series we computed anomalies relative to 1961 to 1990. The
885 uncertainty of mean annual coral Sr/Ca-SST anomalies is indicated by the grey envelope.
886 Potential warm bias in coral SST is indicated in parathenses, pointing up for warm and
887 down for potential cool biases, respectively. Parathenses with inset D marks core interval
888 with diagenesis.

889

890 Figure 3 - Thin-section and SEM images of primary coral aragonite (PA) and aragonite
891 cement (AC) in cores Totor and Cabri. A and B: Excellent preservation of the primary
892 coral aragonite in core Totor. Trace amounts of aragonite cements occur as isolated
893 patches in core sections 6 (C), 7 (D) and 11 (E) of Totor. F (left): A prominent growth
894 break (stippled line) in core section 12 of Totor is encrusted by coralline red algae
895 (CRA). F (middle): The section above the growth break shows well preserved primary
896 coral aragonite. F (right): The pristine coral skeleton of core Cabri contains locally
897 aragonitic sediment (S) partially filling growth-framework pores. A to E: Thin section
898 photographs are shown in plane- (left) and cross-polarized light (middle). F: All thin
899 section photographs are shown in plane-polarized light.

900

901 Figure 4 – a) Climatology at Rodrigues between 1997 to 2007. Monthly averaged SST *in*
902 *situ* (red), ERSSTv.3b (grey; Smith et al., 2008) and AVHRR SST (blue stippled;
903 Reynolds et al., 2007); b) Reconstructed absolute SST from coral Sr/Ca from cores Totor
904 (dark grey with triangle) and Cabri (light grey with diamond) for 2002 to 2006 based on
905 calibration with *in situ* SST from Rodrigues (red). The uncertainty for single month

906 absolute SST for individual cores Cabri and Totor is 1.23°C and 1.05°C (1σ),
907 respectively. The coral data agree with *in situ* SST within the 1σ uncertainty.

908

909 Figure 5 – Time series of annual mean temperatures anomalies relative to the 1961-1990
910 mean for the coral Cabri SST reconstruction, Rodrigues weather station air temperature
911 (AT), ERSSTv3b, ERSSTv4, HadISST, HadSST3, HadMAT1 and HadNMAT2 for the
912 period 1950 to 2006. The uncertainty of mean annual coral Sr/Ca-SST anomalies is
913 indicated by the grey envelope.

914

915 Figure 6 – a) Monthly interpolated Sr/Ca profiles for cores Cabri (red) and Totor (grey).
916 b) Images of core Totor (coloured blue) with orientation of corallites indicated. Years for
917 core sections indicated on coral slab and grey arrow points to major change in growth
918 pattern in Totor core top section around the years 1983/84.

919

920 Figure 7 – Spatial correlation of Cabri Sr/Ca-SST anomalies (relative to 1961-1990) with
921 HadISST (Rayner et al., 2003). January to March austral summer in a) between 1945-
922 2006, b) 1961-1990 and c) 1971-2006. Annual mean correlations in d) between 1945-
923 2006, e) 1961-1990 and f) 1971-2006. Only correlation with $p < 0.05$ is coloured.
924 Computed at KNMI climate explorer (van Oldenborgh and Burgers, 2005). Yellow star in
925 a) marks location of Rodrigues Island.

926

927 Figure 8 – Spatial correlations of Left) Cabri coral SST and Right) HadISST grid for
928 Rodrigues Island with global austral summer HadISST for a-c) 1950 to 1975 (February to
929 May) negative PDO phase (Mantua et al., 1997) and c-d) 1976 to 1999 (January to April)

930 positive PDO phase. Only correlations with $p < 0.05$ coloured. Computed at KNMI climate
931 explorer (van Oldenborgh and Burgers, 2005). Yellow star in a) marks location of
932 Rodrigues Island.

933

934 Figure 9 – Comparison of Southwestern Indian Ocean (SWIO) coral records from St.
935 Marie Island (black; Grove et al., 2013) with the Cabri record from Rodrigues (red). A
936 SST time series for the grid-box in the SWIO averaged between 12-20°S and 50-63°E is
937 also illustrated (light blue). All time were annualized and converted to SST anomalies
938 relative to 1961-1990. The uncertainty of mean annual Cabri Sr/Ca-SST anomalies is
939 indicated by the grey envelope.

940

941 Figure A1 –Number of SST observations in the grid box surrounding Rodrigues in the
942 ICOADS database. Note the extremely sparse observations even in recent years (van
943 Oldenborgh and Burgers, 2005).

944

945 Figure A2 – Spatial correlations of mean annual HadMAT1 air temperature anomalies
946 between 1945 to 2001 relative to 1961-1990 with a) HadISST for Rodrigues, and b) Cabri
947 SST. Only correlations with $p < 0.05$ coloured. Computed at KNMI climate explorer (van
948 Oldenborgh and Burgers, 2005). Y-axis Latitude, X-axis Longitude.

949

950 Figure A3 – Correlation of the Subtropical Indian Ocean Dipole Mode with global
951 HadISST between 1958 and 2006 for austral summer January to March averages (Behera
952 and Yamagata, 2001; Rayner et al., 2003). Note the location of Rodrigues Island (marked

953 by yellow star) at the northeastern flank of the SIOD and the negative correlations there.
954 Only correlations with $p < 0.05$ coloured. Computed at KNMI climate explorer (van
955 Oldenborgh and Burgers, 2005).

956

957 Figure A4 – X-ray positive print for core sections of core Totor with sampling lines
958 indicated. Blue lines indicate high resolution sampling tracks. Yellow lines superimposed
959 on blue lines indicate sampling at annual resolution for other purposes. Start or end years
960 for each core section indicated.

961

962 Figure A5 - X-ray positive print for core sections of core Cabri with sampling lines
963 (milling holes) indicated. Start or end years for each core section indicated. Note the dead
964 surface before 1907 that is most probably related to a past coral bleaching event.

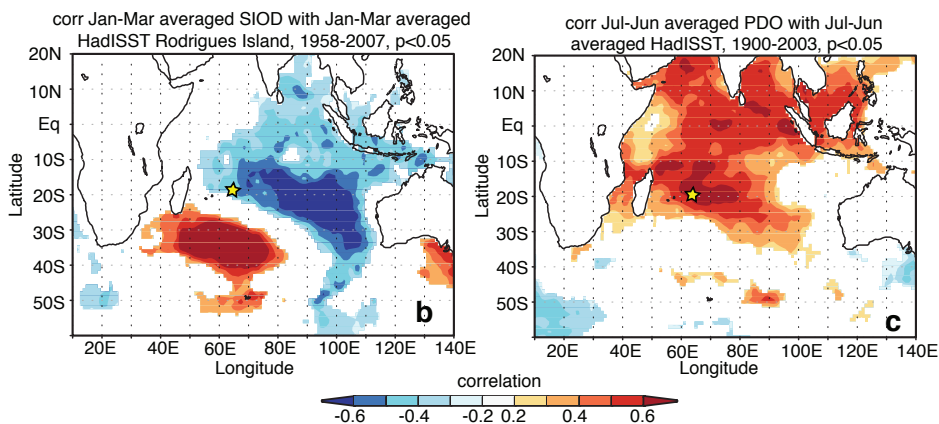
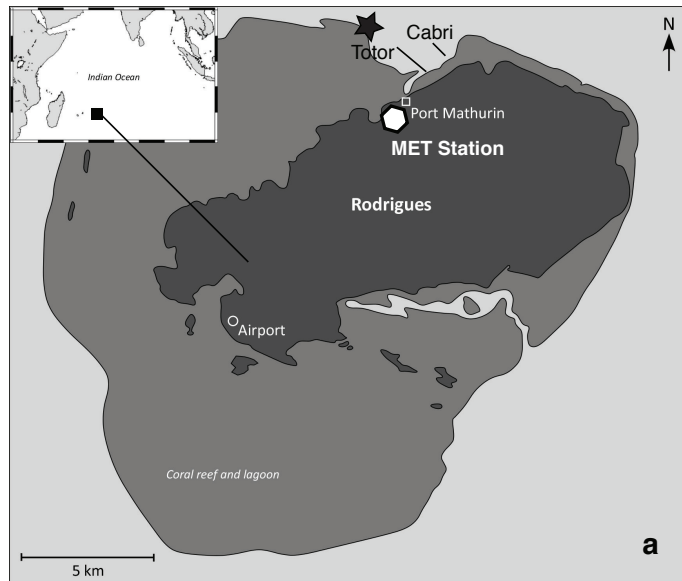
965

966 Table A1 – Statistics of various sea surface temperature (SST) products and air
967 temperature for Rodrigues with 1σ standard deviations in brackets for the period 2002 to
968 2006 (period with *in situ* SST data). STDV = 1σ standard deviation over all years. All
969 units in °C.

970

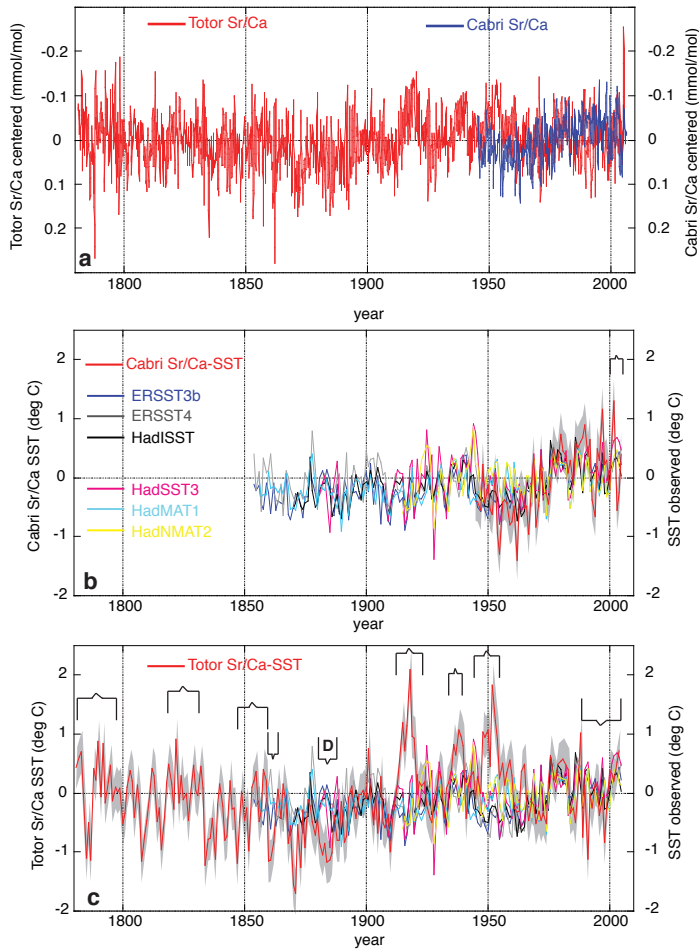
971 Table A2 - Linear regression of coral Sr/Ca with a) *in situ* SST 2002-2005/6, b)
972 ERSSTv.3 (Smith et al., 2008) 1997-2005/6, c) AVHRR SST NOAA Coral Reef watch
973 data 2000-2005/6 and d) monthly Sr/Ca with AVHRR SST (Reynolds et al., 2007) for the
974 period 1982 to 2005.

975

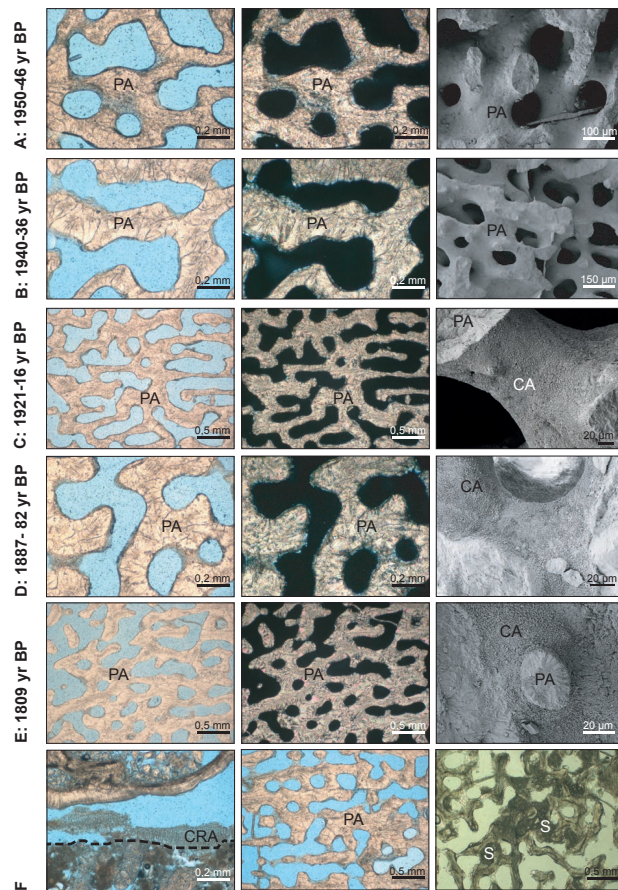


976

977 Figure 1 – a) Map of Rodrigues Island with the position of the two corals cores at Totor
 978 and Cabri indicated. The star shows the position of the CTD that collects SST and salinity
 979 data. Polygon indicates the location of the Meteorological Station which records air
 980 temperature, sunshine hours, wind speed and rainfall. b) Spatial correlation between
 981 January-March averaged SIOD index (Behera and Yamagata, 2001) with HadISST
 982 (Rayner et al., 2003) for Rodrigues Island. c) Spatial correlation between July-June mean
 983 annual averaged PDO index (Mantua et al., 1997) with HadISST (Rayner et al., 2003).
 984 All correlations with detrended data. Only correlation with $p < 0.05$ are coloured.
 985 Computed at KNMI climate explorer (van Oldenborgh and Burgers, 2005). Yellow star in
 986 b) and c) marks the location of Rodrigues Island.



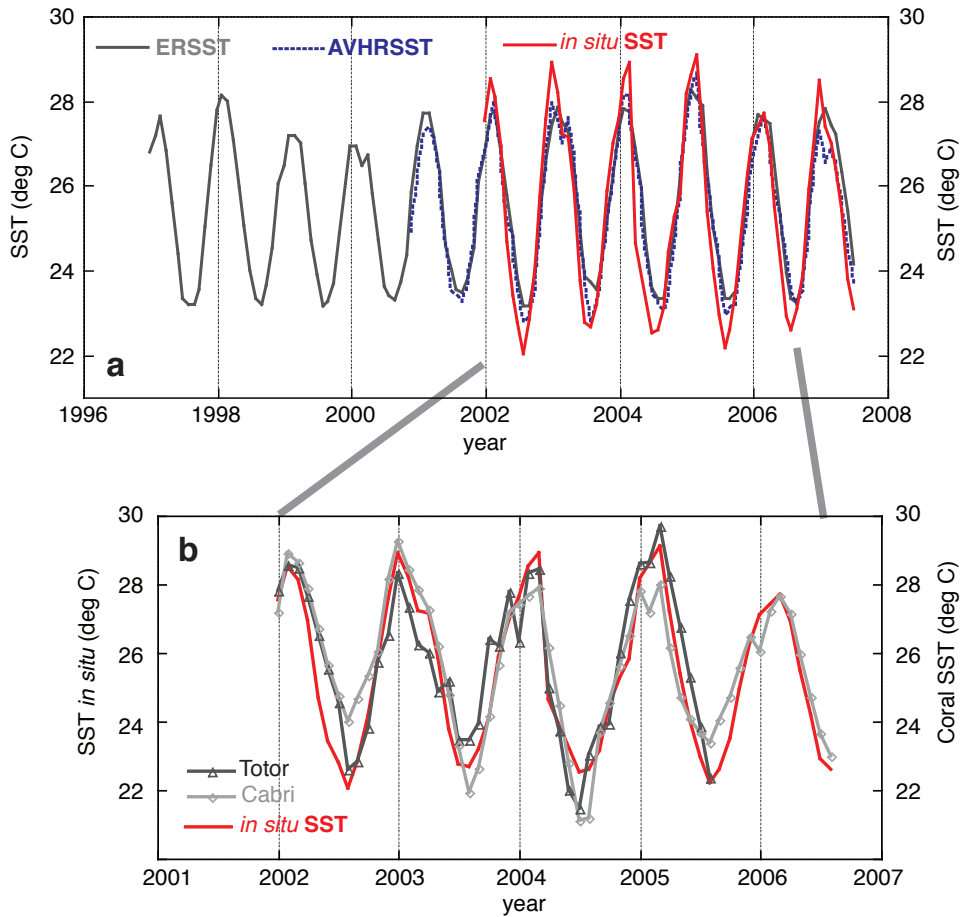
987
 988 Figure 2 - a) Time series of monthly (thin solid lines) Sr/Ca anomalies (right Y-axis
 989 converted) relative to the 1961 to 1990 climatological mean for coral cores Cabri (top),
 990 Totor (middle) for the period 1781 to 2006. Annual mean time series of individual cores
 991 (red line) b) Cabri and c) Totor compared to SST reconstructions: ERSSTv3b, ERSSTv4,
 992 HadISST, HadSST3, HadMAT1 and HadNMAT2. See legend in b) and c) for colour
 993 code. For all time series we computed anomalies relative to 1961 to 1990. The
 994 uncertainty of mean annual coral Sr/Ca-SST anomalies are indicated by the grey
 995 envelope. Potential warm bias in coral SST is indicated by brackets, pointing up for warm
 996 and down for potential cool biases, respectively. Bracket with inset D marks core interval
 997 with diagenesis.
 998



999

1000 Figure 3 - Thin-section and SEM images of primary coral aragonite (PA) and aragonite
 1001 cement (AC) in cores Totor and Cabri. A and B: Excellent preservation of the primary
 1002 coral aragonite in core Totor. Trace amounts of aragonite cements occur as isolated
 1003 patches in core sections 6 (C), 7 (D) and 11 (E) of Totor. F (left): A prominent growth
 1004 break (stippled line) in core section 12 of Totor is encrusted by coralline red algae
 1005 (CRA). F (middle): The section above the growth break shows well preserved primary
 1006 coral aragonite. F (right): The pristine coral skeleton of core Cabri contains locally
 1007 aragonitic sediment (S) partially filling growth-framework pores. A to E: Thin section
 1008 photographs are shown in plane- (left) and cross-polarized light (middle). F: All thin
 1009 section photographs are shown in plane-polarized light.

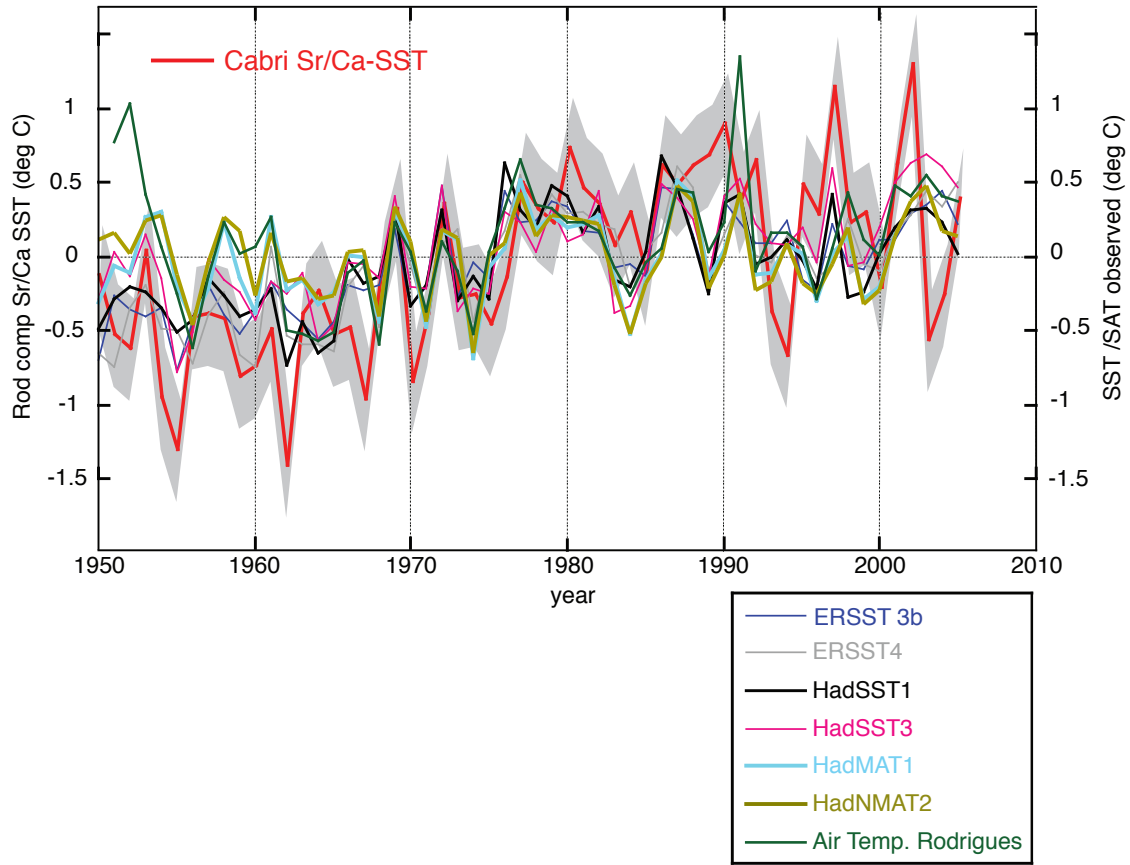
1010



1011

1012 Figure 4 – a) Climatology at Rodrigues between 1997 to 2007. Monthly averaged SST
1013 *in situ* (red), ERSSTv.3 (grey; Smith et al., 2008) and AVHRR SST (blue stippled;
1014 Reynolds et al., 2007); b) Reconstructed absolute SST from coral Sr/Ca from cores Totor
1015 (dark grey with triangle) and Cabri (light grey with diamond) for 2002 to 2006 based on
1016 calibration with *in situ* SST from Rodrigues (red). The uncertainty for single month
1017 absolute SST for individual cores Cabri and Totor is 1.23°C and 1.05°C (1σ),
1018 respectively. The coral data agree with *in situ* SST within the 1σ uncertainty.

1019

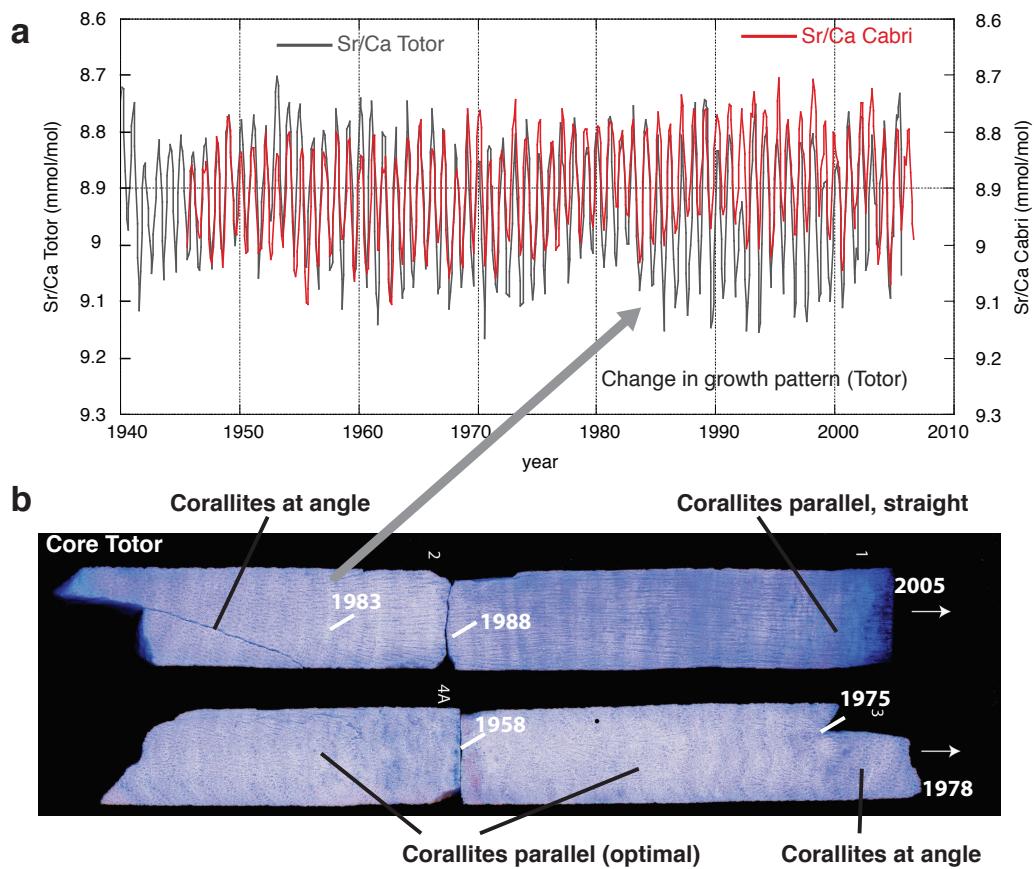


1020

1021 Figure 5 – Time series of annual mean temperatures anomalies relative to the 1961-1990
 1022 mean for the coral Cabri SST reconstruction, Rodrigues weather station Air temperature
 1023 (AT), ERSSTv3b, ERSSTv4 , HadISST, HadSST3, HadMAT1 and HadNMAT2 for the
 1024 period 1950 to 2006. The uncertainty of mean annual coral Sr/Ca-SST anomalies are
 1025 indicated by the grey envelope.

1026

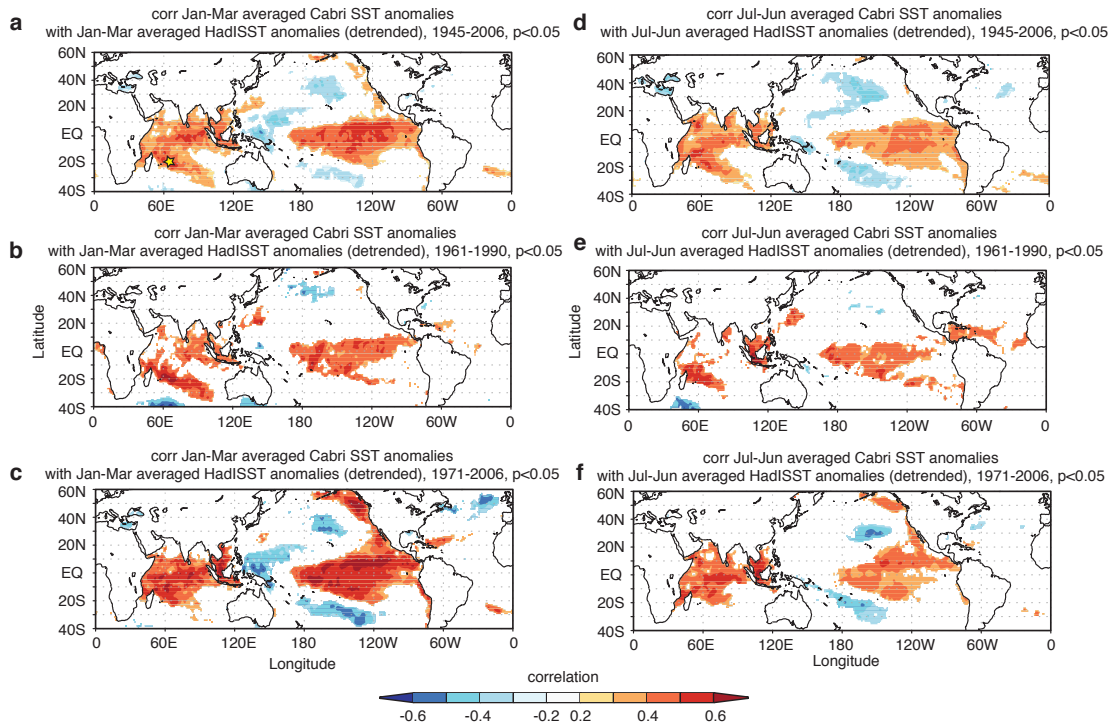
1027



1028

1029 Figure 6 – a) Monthly interpolated Sr/Ca profiles for cores Cabri (red) and Totor (grey).
 1030 B) Images of core Totor (coloured blue) with orientation of corallites indicated. Years for
 1031 core sections indicated on coral slab and grey arrow points to major change in orientation
 1032 of corallites in core top section of Totor around 1983/84.

1033

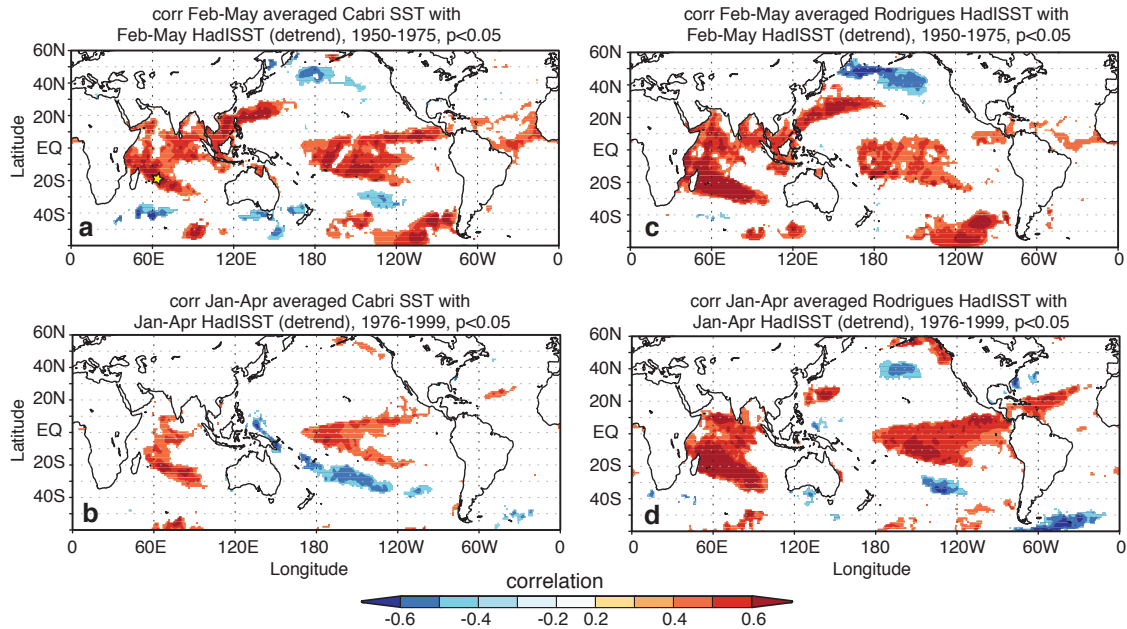


1034

1035 Figure 7 – Spatial correlation of Cabri Sr/Ca-SST anomalies (relative to 1961-1990) with
 1036 HadISST (Rayner et al., 2003). January to March austral summer in a) between 1945-
 1037 2006, b) 1961-1990 and c) 1971-2006. Annual mean correlations in d) between 1945-
 1038 2006, e) 1961-1990 and f) 1971-2006. Only correlation with $p < 0.05$ are coloured.
 1039 Computed at knmi climate explorer (van Oldenborgh and Burgers, 2005). Yellow star in
 1040 a) marks location of Rodrigues Island.

1041

1042

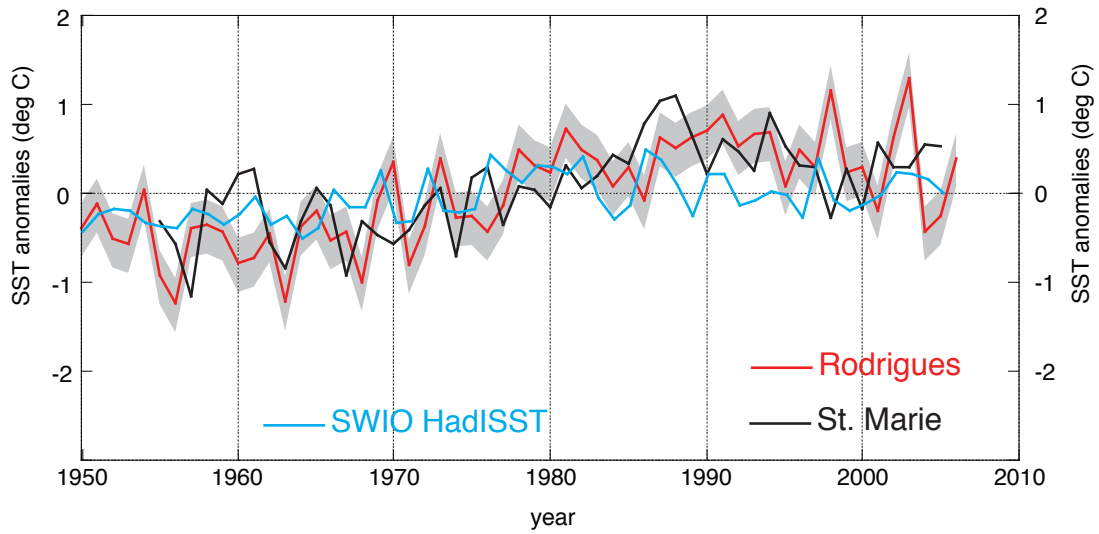


1043

1044 Figure 8 – Spatial correlations of Left) Cabri coral SST and Right) HadISST grid for
 1045 Rodrigues Island with global austral summer HadISST for a-c) 1950 to 1975 (February to
 1046 May) negative PDO phase (Mantua et al., 1997) and c-d) 1976 to 1999 (January to April)
 1047 positive PDO phase. Only correlations with $p < 0.05$ coloured. Computed at knmi climate
 1048 explorer (van Oldenborgh and Burgers, 2005). Yellow star in a) marks location of
 1049 Rodrigues Island.

1050

1051



1052

1053 Figure 9 – Comparison of southwestern Indian Ocean (SWIO) coral records from St.
 1054 Marie Island (black; Grove et al., 2013) with the Cabri record from Rodrigues (red). An
 1055 SST time series for the grid-box in the SWIO averaged between 12-20°S and 50-63°E is
 1056 also illustrated (light blue). All time were annualized and converted to SST anomalies
 1057 relative to 1961-1990. The uncertainty of mean annual Cabri Sr/Ca-SST anomalies are
 1058 indicated by the grey envelope.

1059

1060

1061

1062

1063

1064

1065

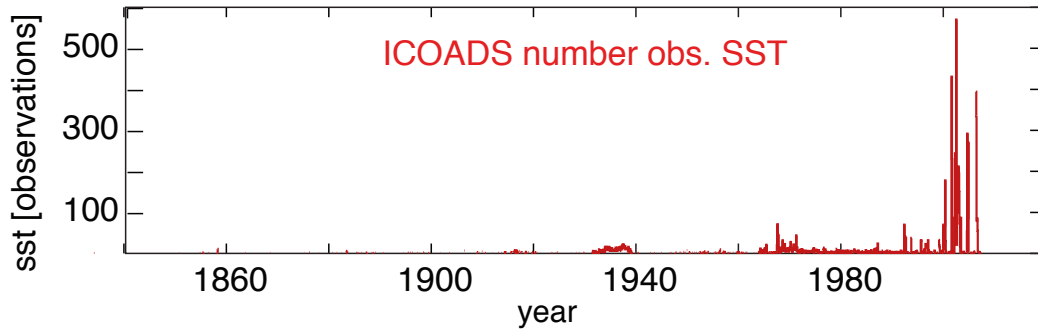
1066

1067

1068

1069 **Appendix A –Instrumental sea surface temperature (SST) records and linear**
1070 **regression equations of coral Sr/Ca with SST.**

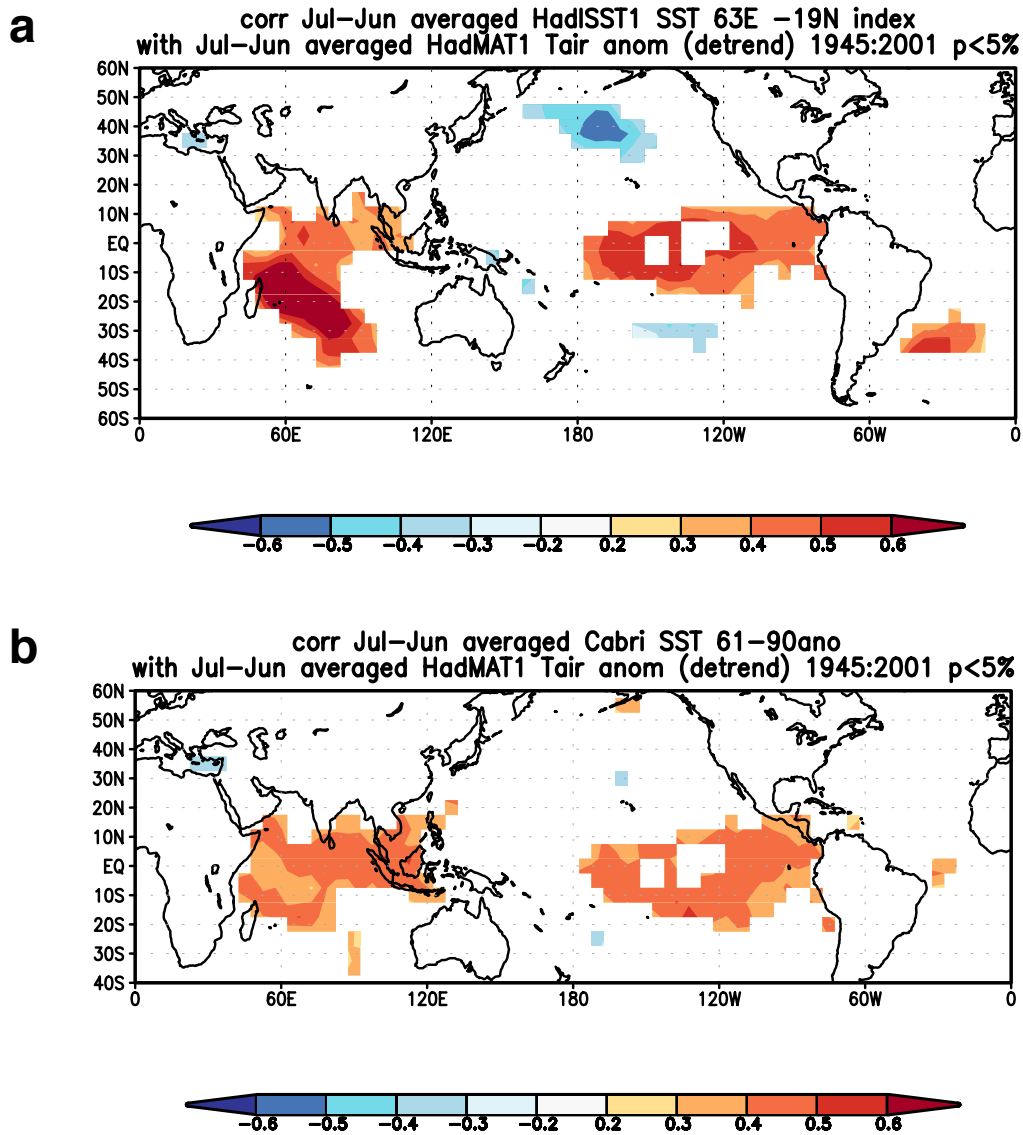
1071



1072

1073 Figure A1 –Number of SST observations in the grid box surrounding Rodrigues in the
1074 ICOADS database. Note the extremely sparse observations even in recent years (van
1075 Oldenborgh and Burgers, 2005).

1076



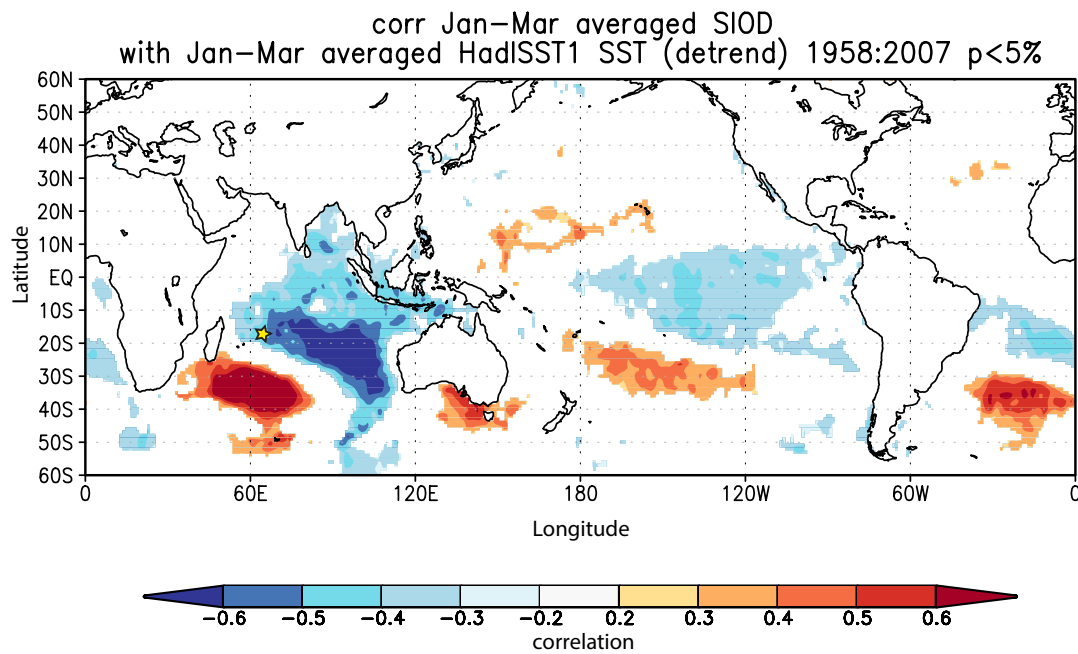
1077

1078 Figure A2 – Spatial correlations of mean annual HadMAT1 air temperature anomalies
 1079 between 1945 to 2001 relative to 1961-1990 with a) HadISST for Rodrigues, and b) Cabri
 1080 SST. Only correlations with $p < 0.05$ coloured. Computed at knmi climate explorer (van
 1081 Oldenborgh and Burgers, 2005). Y-axis Latitude, X-axis Longitude.

1082

1083

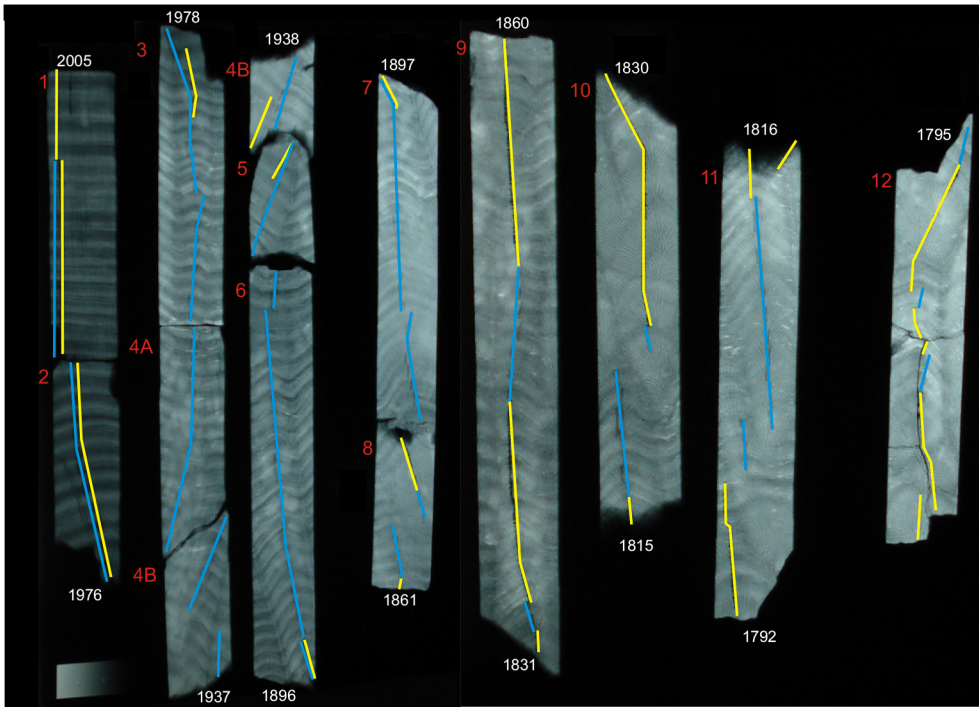
1084



1085

1086 Figure A3 – Correlation of the Subtropical Indian Ocean Dipole Mode with global
 1087 HadISST between 1958 and 2006 for austral summer January to March averages (Behera
 1088 and Yamagata, 2001; Rayner et al., 2003). Note the location of Rodrigues Island (marked
 1089 by yellow star) at the northeastern flank of the SIOD and the negative correlations there.
 1090 Only correlations with $p < 0.05$ coloured. Computed at knmi climate explorer (van
 1091 Oldenborgh and Burgers, 2005).

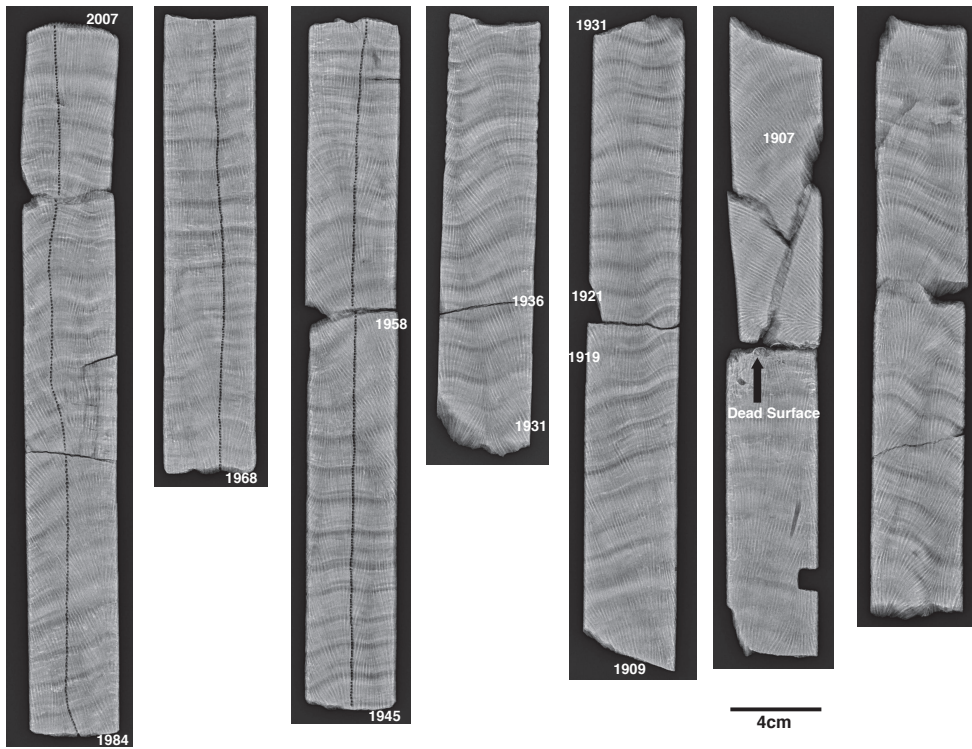
1092



1093

1094 Figure A4 – X-ray positive print for core sections of core Totor with sampling lines
 1095 indicated. Blue lines indicate high resolution sampling tracks. Yellow lines superimposed
 1096 on blue lines indicate sampling at annual resolution for other purposes. Start or end years
 1097 for each core section indicated.

1098



1099

1100 Figure A5 - X-ray positive print for core sections of core Cabri with sampling lines
 1101 (milling holes) indicated. Start or end years for each core section indicated. Note the dead
 1102 surface before 1907 that is most probably related to a past coral bleaching event.

1103

1104

1105

1106

1107

1108

1109

1110

1111

	SST <i>in situ</i> 2002-2006	AVHRR SST 2002-2006	ERSST 2002-2006	Air Temp. 2002-2006
Mean annual	25.49 (0.24)	25.4 (0.11)	25.57 (0.3)	27.49 (0.31)
Maximum	28.6 (0.5)	28.65 (0.44)	28.29 (0.4)	31.2 (0.62)
Minimum	22.4 (0.27)	22.75 (0.21)	23.15 (0.13)	24.2 (0.44)
Seasonal Range	6.22 (0.68)	5.9 (0.58)	5.14 (0.39)	7.0 (0.79)
STDV	2.14	1.78	1.69	2.07

1112

1113 Table A1 – Statistics of various sea surface temperature (SST) products and air
1114 temperature for Rodrigues with 1σ standard deviations in brackets for the period 2002 to
1115 2006 (period with *in situ* SST data). STDV = 1σ standard deviation over all years. All
1116 units in °C.

1117

1118

1119

1120

1121

1122

1123

1124

1125

1126

1127

1128

(a) Max-Min	Regression equation	r²	p
Totor	Sr/Ca = -0.0439(±0.004)*SST + 10.032(±0.10)	0.97	<0.001
Cabri	Sr/Ca = -0.0384(±0.005)*SST + 9.861(±0.12)	0.89	<0.001
(b) Max-Min			
Totor	Sr/Ca = -0.0638(±0.004)*SST + 10.566(±0.09)	0.95	<0.001
Cabri	Sr/Ca = -0.0507(±0.004)*SST + 10.179(±0.10)	0.90	<0.001
(c) Max-Min			
Totor	Sr/Ca = -0.0531(±0.004)*SST + 10.271(±0.11)	0.96	<0.001
Cabri	Sr/Ca = -0.0441(±0.005)*SST + 10.012(±0.13)	0.88	<0.001
(d) Monthly			
Totor	Sr/Ca = -0.0522(±0.003)*SST + 10.272(±0.08)	0.79	<0.001
Cabri	Sr/Ca = -0.0419(±0.003)*SST + 9.95(±0.07)	0.87	<0.001

1129

1130 Table A2 - Linear regression of coral Sr/Ca with a) *in situ* SST 2002-2005/6, b)
 1131 ERSSTv.3 (Smith et al., 2008) 1997-2005/6, c) AVHRR SST NOAA Coral Reef watch
 1132 data 2000-2005/6 and d) monthly Sr/Ca with AVHRR SST (Reynolds et al., 2007) for the
 1133 period 1982 to 2005.

1134

1135